RESOLUTION OF ISOTROPIC PERCENTAGE IN MOMENT TENSOR INVERSION OF TENSILE SOURCES

by

Gökçe Öter

B.S. Geophysical Engineering, İstanbul University, 2015

Submitted to the Kandilli Observatory and Earthquake Research Institute in partial fulfillment of the requirements for the degree of Master of Science

Graduate Program in Geophysics

Boğaziçi University

2019

ACKNOWLEDGEMENTS

Foremost, I would like to thank my thesis advisor Assoc. Prof. Dr. Çağrı Diner of the Geophysics Department at Boğaziçi University for the continuous support of my MSc study and research. His guidance helped me all the time in researching and writing process of this thesis.

I would also like to thank Assoc. Prof. Dr. Ali Özgün Konca of the Geophysics Department at Boğaziçi University especially for his guidance in the data process problems that I faced while doing this study.

Finally, I would like to thank my parents for their encouragement and incredible support both spiritually and materially. I would also like to thank my classmates and Sezim Güvercin for their technical help and insightful comments. Without their supports, this thesis would not have been completed. Thank you.

ABSTRACT

RESOLUTION OF ISOTROPIC PERCENTAGE IN MOMENT TENSOR INVERSION OF TENSILE SOURCES

Moment tensor solutions are commonly used in order to understand earthquake source mechanism. Moment tensor can be decomposed into three components, namely isotropic (ISO), double-couple (DC) and compensated linear vector dipole (CLVD). It is well-known fact that tensile sources generate non-DC components and those earthquakes can be defined as the combination of both tensile and shear motion on a fault. In this thesis, resolution of the isotropic part in the moment tensor are considered for tensile sources. For that reason, synthetic waveforms are created by using full moment tensors with different isotropic percentages and those waveforms are inverted with gCAP method. Afterwards, a range of different isotropic values, with a step of $t = 0.1$, are forced in the moment tensor inversion process in order to investigate the change in variance reduction as the isotropic percentage deviate from its true value. Inversions of the full waveform are performed in different distances and depths for three moment tensors with different isotropic percentages, namely 2%, 5% and 14%. Inversions results of those original moment tensors and moment tensors with manipulated isotropic percentages are expressed. Those results are compared to each other in terms of changing isotropic percentages, depth and variance reduction in different stations.

The results can be summarized as firstly, inversion is not really sensitive to the isotropic component of the moment tensor because isotropic component has small energy compared to the whole waveform. Secondly, earthquakes with relatively high isotropic percentages are less sensitive when inversions are performed for high values of manipulated isotropy. Finally, it is observed that the error in the depth of the earthquake is very sensitive to isotropic percentage.

ÖZET

AÇILMA KAYNAKLARI İÇİN MOMENT TENSÖR İÇERİSİNDEKİ İZOTROPİK KISMIN ÇÖZÜNÜRLÜĞÜ

Moment tensör çözümleri, depremlerin kaynak mekanizmasını anlamak için yaygın olarak kullanılmaktadır. Moment tensör özgün olarak üç farklı parçaya ayrılabilir; izotropik (ISO), çift kuvvet (DC) ve çizgisel vektör dipolü (CLVD). Açılma kaynaklarının DC olmayan bileşenler ürettiği ve bu depremlerin bir fay üzerinde hem açılma hem de kayma hareketinin birleşimi olarak tanımlanabileceği bilinen bir durumdur. Bu tez çalışmasında, açılma depremleri için moment tensor içerisindeki izotropik kısmın çözünürlügü ele alınmıştır. Bu nedenle, farklı izotropi yüzdelerine sahip depremler üretilmiş ve bu depremleri temsil eden moment tensörlerin gCAP yöntemiyle ters çözümleri yapılmıştır. Bununla birlikte, izotropi bileşeninin moment tensöründeki çözünürlüğünü anlamak için ters çözüm aşamasında izotropi değerleri, 0.1 aralıklarla farklı izotropi değerleriyle manipüle edilmiştir. Tam dalga formunun ters çözümü, farklı izotropik yüzdelere sahip üç farklı moment tensör (2%, 5% ve 14%) için farklı mesafelerde ve derinliklerde hesaplanmıştır. Orjinal moment tensörler ve izotropi değeri değiştirilmiş moment tensörlerin ters çözümleri gösterilmiş ve bu sonuçlar farklı istasyonlarda, farklı derinliklerde ve varyans azaltılması açısından kendi aralarında mukayese edilmiştir.

Sonuçlar şu şekilde özetlenebilir; ilk olarak, moment tensörün ters çözümü izotropiye gerçekten duyarlı değildir, çünkü izotropi bileşeni tüm dalga formuna kıyasla küçük miktar enerjiye sahiptir. Yüksek izotropi yüzdelerine sahip olan depremler, değiştirilmiş izotropinin yüksek değerleri için ters çözümler yapıldığında daha az hassastır. Son olarak, deprem derinliğindeki hatanın izotropik yüzdeye çok duyarlı olduğu gözlenmiştir.

TABLE OF CONTENTS

LIST OF FIGURES

LIST OF TABLES

LIST OF SYMBOLS/ABBREVIATIONS

A	Fault area (km^2)
C_{ijpq}	Elasticity tensor
D	Slip of a fault (cm)
d	Source tensor
d^{iso}	Isotropic part of the source tensor
d^{dev}	Deviatoric part of the source tensor
f_i	Interior body force
G_{ni}	Green's Function
$G_{nk,l}$	Moment Tensor Green's function
I	Identity matrix
I_{ij}	Normalized isotropic tensor
M_{kl}	Moment tensor
M_0	Seismic moment
M_w	Moment magnitude
M^*	Deviatoric moment
m	Moment density function
n	Fault normal
P	Potency
P_0	Scalar potency
P_{ij}	Seismic potency tensor
tr(M)	Trace of a matrix M
u	Slip vector
u_n	Displacement at the receiver
V	Domain (km^2)
x	Location of reciever
α	Angle between slip and fault plane
δ	Dip Angle of a fault plane
δ_{ij}	Kronecker delta.

ϵ_{kl}	Strain tensor
ϵ	Epsilon
ζ	Isotropic parameter of moment tensor
ζ_p	Strength of the isotropic part for the potency tensor
η	Poisson's ratio
λ	Rake angle of a fault plane
λ	Elasticity modulus
λ_1^c	Eigenvalue of isotropic tensor
λ_2^c	Eigenvalue of deviatoric tensor
μ	Rigidity
ξ	Location of a Source
ρ	Mass of a material
Σ	Fault Region
σ_{ij}	Stress Tensor
τ	Source Time
ϕ	Strike Angle of a Fault Plane
χ	CLVD parameter of moment tensor
χ_p	Strength of the CLVD part for the potency tensor

LIST OF ABBREVIATIONS

1D	One Dimensional
2D	Two Dimensional
3D	Three Dimensional
6D	Six Dimensional
CLVD	Compensated Linear Vector Dipole
DC	Double Couple
ISO	Isotropic
non-DC	non double couple
TI	Transversely Isotropic

1. INTRODUCTION

Moment tensor solutions are commonly used in order to understand source mechanism. Full moment tensor inversions have become more important now for understanding the mechanisms of earthquakes as the resolution of the inversion process increases.

Besides the double couple (DC) component of moment tensor, which is frequently encountered in the solution of tectonic earthquakes, some sources can generate non double couble (non-DC) components as well. Vavrycuk (2011) states that tensile earthquakes are the combination of shear and tensile motions on a fault [1]. When the slip of the plane is not perpendicular to the normal vector of the plane, it generates non double couple components such as shallow earthquakes in volcanic or geothermal regions [1].

In the article of Alvizuri and Tape's (2016), the full moment tensor inversions and solutions are studied in order to understand the structure of real events in geothermal fields, volcanic fields, mines, oil fields or induced earthquakes [2]. Moment tensors in geothermal and volcanic fields are mainly considered in their article because non-tectonic earthquakes have relatively more non double couple character [2]. In the literature, there are a lot of different moment tensor solutions using different inversion methods (first motion polarity, body wave, surface wave, waveform difference, amplitude ratio) and different frequency ranges are also considered. Pesicek et. al. (2012) states that it is hard to identify phase arrivals in a correct way when a signal has noise and station are placed at the close range to the source [3]. For that reason, in this thesis station distances are considered in order to distinguish phase arrivals separately. Futhermore, Panza et. al. (2000) also states that structural velocity model may be the reason of considerable noise in the data, therefore, we use one layer half-space velocity model in order to reduce possible noise in the waveforms [4].

The main emphasis is examined in many different cases when performing the full moment tensor solution and inversion. In Alvizuri and Tape's (2016) article, small-magnitude earthquakes and even micro earthquakes are considered, so different station numbers and distances are also considered [2]. In general, isotropy only exists in P wave and relatively small amount in the full wave, for that reason, more and close stations are needed. Alvizuri and Tape's (2016) also states that moment tensor is an increasingly common method, but there are some reservations about its sensitivity, especially about the isotropic component resolution [2].

The main purpose of this study is exploring the tensile earthquakes, and investigating what kind of criteria should be taken into consideration in the inversion process to obtain reliable results. For that reason, three different synthetic earthquakes with different isotropic percentages,namely 2%, 5%, 14%, are considered and it is aimed to find if the resolution of isotropic components differs in those cases. Those earthquakes are recorded at sets of stations with different distances. In this thesis, waveforms of synthetic earthquakes with different isotopic percentages are shown and inversions of moment tensors from those synthetic waveforms are also considered.

In chapter 2, the elastodynamic equation is derived by using Hooke's law. Then its Green's function solution is stated which is known as representation theorem. In this solution, the moment tensor expression is obtained and it is shown that data and moment tensor are linearly related. Afterwards, decomposition of the moment tensor is mentioned in order to calculate the isotropic percentage.

Chapter 3 describes the moment, elasticity and source tensors expressions in Kelvin notation in order to use the linear algebraic manipulation tools for the decomposition. Characterization of the tensile sources in the isotropic focal region is defined. Additionally, strain-based potency tensor and its isotropic and deviatoric components are represented similar to moment tensor decomposition. Moreover, isotropic parameters ζ for the moment tensor and ζ_p for the potency tensor are also derivated. Inversion theory and application method of the inversion (gCAP) for this study are also mentioned at the end of the chapter.

Chapter 4 includes the applications of the method. First, data set and its conditions are introduced. Distribution of the stations with respect to source location are represented. Inversions are performed in different distances and depths for three different moment tensors, which has different percentage of isotropy namely 2%, 5%, 14%. This process is approached as a case study. Apart from the original results of the inversions, manipulated inversions results are also considered. As a result of those inversions, changes in the strike, rake and dip angles with respect to manipulated percentages of ISO are shown. We conclude this chapter by representing the manipulated inversion results for different hypocentral depths of the earthquakes.

In the last chapter, the results are discussed and compared to each other in terms of changing isotropic percentages, depth, variance reduction and waveforms in distributed stations. In this section, comparison of the inversions results for three different synthetic earthquakes with different isotropic percentages,namely 2%, 5%, 14% are mainly considered. Different stations sets are used in order to perform those inversions for different earthquakes. There are totally 10 stations for each set, which are located at 15, 45 and 80 km far away from the source. Firstly, isotropic component in the full waveforms of different earthquakes are compared. Afterwards, inversion results of moment tensors with different isotropic percentages are compared for different stations distances. Thirdly, earthquakes with different isotropic component are also compared for the same stations. Finally, the hypocentral depths of the original earthquakes are changed in order to observe changes in isotropic perentage and variance reduction values as a result of inversions.

2. THEORETICAL BACKGROUND

In this chapter, theoretical background of this research is introduced. In particular, the definitions of the fault plane parameters, equivalent body forces, Green's function, elasticity tensor, moment tensor decomposition and representation theorem are stated.

2.1. Equation of Motion

By using Newton's second law, equation of motion can be written. The total force of a material is equal to the mass of a material (ρ) multiplied by acceleration ($\ddot{u}_i$) (double differentiation of displacement with respect to time). Interior body forces f_i and surface forces, which are represented by stress tensor σ_{ij}, are the two types forces acting on a particle in a continuum.

Consequently, the equation 2.1 that represents elastic motion in a continuum can be written by using Einstein's summation convention as

$$\rho(\mathbf{x})\ddot{u}_i = f_i + \sigma_{ij,j}, \qquad i \in \{1, 2, 3\}, \tag{2.1}$$

where u denotes the displacement and the two dots above u denotes the second derivative of displacement, namely acceleration. In order to write down equation 2.1 as a partial differential equation with respect to the unknown function $\mathbf{u}$, we are going to write down stress tensor σ_{ij} in terms of displacement. To do so, first we need to express strain as a function of $\mathbf{u}$. The measure of deformation (strain), which is a second rank tensor, depends on differentiation of displacement as

$$\varepsilon_{kl} = \frac{1}{2}(u_{k,l} + u_{l,k}), \tag{2.2}$$

where ε_{kl} is the strain tensor.

2.2. Elasticity Tensor

Elasticity is the attitude of an object to get back its original form when it is being subjected to a stress. The linear relation between elasticity, strain and stress is explained by Hooke's law (in this equation, C_{ijkl} denotes elastic parameters of the medium and it is a fourth rank tensor [26]).

$$\begin{aligned}
\sigma_{ij} &= C_{ijkl}\varepsilon_{ijkl} \\
&= C_{ijkl}\frac{1}{2}(u_{k,l} + u_{l,k}), \\
&= \frac{1}{2}(C_{ijkl}u_{k,l} + C_{ijkl}u_{k,l}), \\
&= \frac{1}{2}(C_{ijkl}u_{k,l} + C_{ijlk}u_{k,l}), \qquad \text{since } C_{ijkl} = C_{ijlk}. \\
&= C_{ijkl}u_{k,l}. \qquad (2.3)
\end{aligned}$$

Consequently, if we substitude equation 2.3 onto 2.1, we get elastodynamic wave equation

$$\rho\ddot{u}_i = f_i + C_{ijkl}u_{k,lj}. \qquad (2.4)$$

assuming that $C_{ijkl} = 0$, namely the medium is homogeneous.

2.3. Green's Function Solution of Elastodynamic Wave Equation

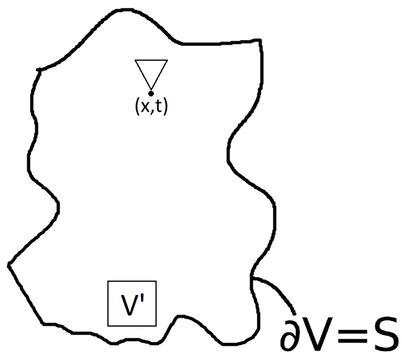

Figure 2.1. V represents the domain, ∂V represents the boundary V′ represents the source area and triangle (x,t) represents the measurement point's location and time.

The vector wave equation, expressed in equation 2.4, has a unique solution if initial and boundary conditions are given as

1. Initial condition for all $x \in V$ $u(x, t_0)$ and $\dot{u}(x, t_0)$
2. A boundary conditions;
   (a) u(x,t) is given for all x ∈ ∂V

   or

   (b) T Traction vector T_i is given, for all $x \in$ ($\mathrm{T}_i = \sigma_{ij} n_j = C_{ijkl} u(x)_{k,l} n_j$).

Therefore, if we admit these initial and boundary conditions as mentioned above, general solution of the vector wave equation can be constructed as

$$\begin{aligned} u_n(x,t) = \int_{-\infty}^{\infty} \iiint_V f_i G_{ni} dV d\tau + \int_{-\infty}^{\infty} \iint_S u_i T_i(G) dS d\tau \\ + \int_{-\infty}^{\infty} \iint_S T_i(u) G_{ni} dS d\tau. \end{aligned} \tag{2.5}$$

The first term in equation 2.5 will result in displacement due to body force. Apart from first term in the equation 2.5, other terms will give us boundary's contribution to displacement.

2.4. Greens's Function Solution for Faults

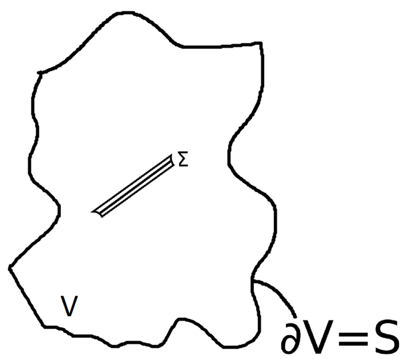

Figure 2.2. Representation theorem for faults. Σ represents the fault region. V is the domain volume and dV is the boundary of the domain.

Assuming that the body source is zero, a fault can be defined as an internal boundary where traction is continuous and displacement is discontinuous. One can use the notation $[u_i] = u_i^+(x,t) - u_i^-(x,t)$ in order to explain the slip discontinuity at the fault surface. Since traction in equation 2.5 is continous the third term in equation 2.5 will vanish for internal boundary Σ which represents the fault region in Figure 2.2, ξ represents the location in the fault region and τ denotes the time of the source, whereas (x,t) represents receiver's location and time[26]. From now on, writing down $T_i(\sigma)$ in terms of displacement, equation 2.5 becomes

$$u_n(x,t) = \int_{-\infty}^{\infty} \iint_{\Sigma} [u_i](\xi,\tau) C_{ijkl} \hat{n}_j \frac{\partial G_{nk}}{\partial \Sigma_l}(x,t;\xi,\tau) d\Sigma d\tau. \tag{2.6}$$

Because of the shifting property of Green's function due to time, one can change the time variables. The difference between time at the measurement point and source time is t–τ.

$$G_{ni}(x,t;\xi,\tau) = G_{ni}(x,t-\tau;\xi,0) \tag{2.7}$$

If the Green's function is represented in the right side of equation 2.7, time integral can be assumed as a convolution.

$$f(t) * g(t) = \int_{-\infty}^{\infty} f(\tau) g(t-\tau) d\tau. \tag{2.8}$$

Then 2.4 becomes,

$$u_n(x,t) = \iint_{\Sigma} [u_i](\xi,\tau) C_{ijkl} \hat{n}_j * G_{nk,l}(x,t;\xi,\tau) d\Sigma_{(\xi)}. \tag{2.9}$$

2.5. Equivalent Body Forces

To get the equivalent body forces, Green's function should be vanished from the equation 2.9. By integrating the slip on the fault plane equation 2.9 proceeds the displacement at a measurement point. By adding a dirac delta term to the equation, volume integral for the whole area can be written in place of integral that is only for the fault region. The spacial variable for source ξ will become to η.

$$u_n(x,t) = \iiint_V ([u_i](\xi,\tau)C_{ijkl}\hat{n}_j\delta(\Sigma)) * G_{nk,l}(x,t;\xi,\tau)dV_{(\eta)} \tag{2.10}$$

Using partial integration, one can get rid of Green's function's derivative. Green's function vanishes when it is evaluated with the dirac delta at the boundaries, for that reason first term will become zero ($\partial(\Sigma)$ is zero at ∂V outer surface of V), so we can write the equation as

$$u_n(x,t) = -\iiint_V \frac{\partial}{\partial\eta_l}([u_i](\xi,\tau)C_{ijkl}\hat{n}_j\delta(\Sigma)) * G_{nk}(x,t;\eta,\tau)dV_{(\eta)}. \tag{2.11}$$

Consequently, the term $\frac{\partial}{\partial\eta_l}[([u_i](\xi,\tau)C_{ijkl}\hat{n}_j\delta(\Sigma))]$ is the equivalent body force for the fault. And the term $[u_i](\xi,\tau)C_{ijkl}\hat{n}_j$ equals to moment tensor M_{kl}. Then, we can we say that equivalent body force for an earthquake equals to divergence of moment tensor ($M_{kl,l} = \nabla \cdot M_{kl}$).

2.6. Moment Tensor

Equivalent body forces of seismic sources can describe moment tensor represented by M (Figure 2.3). Moment tensor can be explained by two terms, which are fault orientation and source strength.

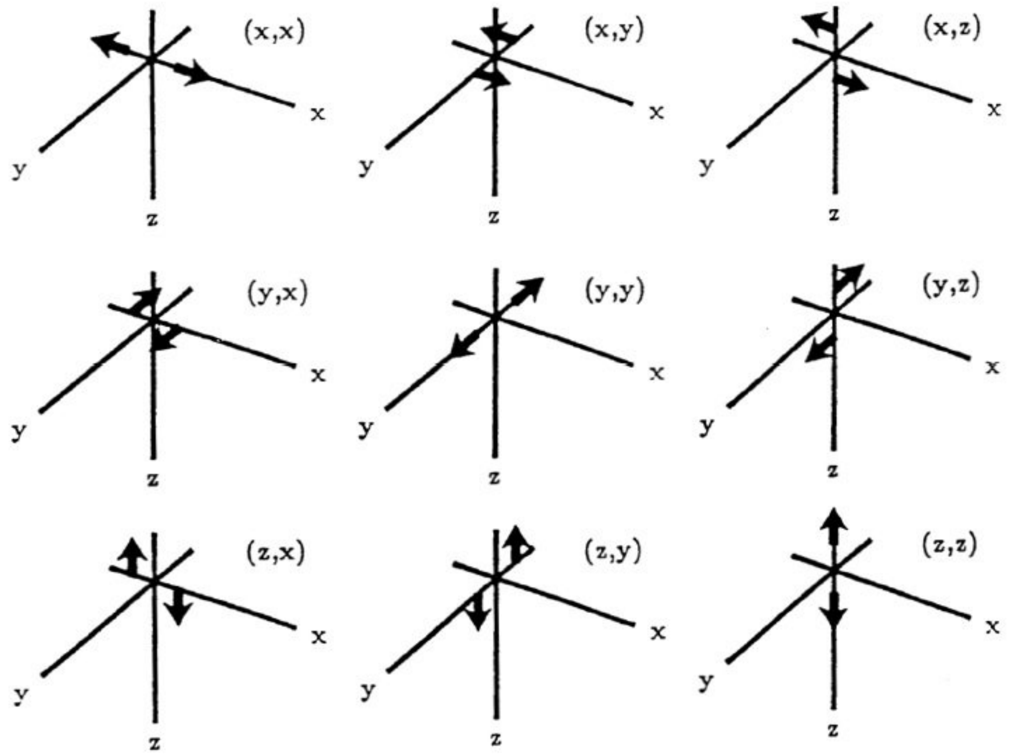

Figure 2.3. General representation of nine force couples.

2.6.1. Moment Density Tensor and Point Source Assumption

Initially, moment density tensor **m** should be explained in order to identify the forces in Figure 2.3 With the help of Green's function solution in the representation theorem, displacement at the receiver $u_n(x,t)$ can be written as below,

$$u_n(\mathbf{x},t) = \iint_{\Sigma} [u_i(\xi,\tau)]\, \hat{n}_j(\xi) C_{ijkl}(\xi) * G_{nk,l}(\mathbf{x},t;\xi,\tau)\, d\Sigma, \tag{2.12}$$

Since the term $[u_i(\xi,\tau)]\, \hat{n}_j(\xi) C_{ijkl}(\xi)$ represents the strength of the (k,l) couple and the term $G_{nk,l}(\mathbf{x},t;\xi,\tau)$ represents the Green's function displacement due to the unit impulse at the source point and time, moment density tensor m_{kl} can be defined as

$$m_{kl} = [u_i(\xi,\tau)]\, \hat{n}_j C_{ijkl}. \tag{2.13}$$

In point of fact, signal is generally used at certain periods for which the whole surface Σ is efficiently a point source. In that case, the radiated waves from the different parts of surface $d\Sigma$ are approximately in phase [26]. In short, whole surface Σ can be assumed as a point, which is the midpoint of Σ. In this manner, by using convolution of moment density tensor at particular points of the fault surface with the Green's function where the source point is fixed, equation 2.13 can be written as

$$\begin{aligned} u_n(\mathbf{x},t) &= \iint_\Sigma [u_i(\xi,\tau)]\, \hat{n}_j(\xi) C_{ijkl}(\xi) * G_{nk,l}(\mathbf{x},t;\bar{\xi},\tau)\; d\Sigma, \\ &= \left(\iint_\Sigma [u_i(\xi,\tau)]\, \hat{n}_j(\xi) C_{ijkl}(\xi)\; d\Sigma \right) * G_{nk,l}(\mathbf{x},t;\bar{\xi},\tau), \end{aligned} \tag{2.14}$$

where $\bar{\xi}$ can be taken as the centroid of the earthquake and the Green's function can be withdrawn from the integral. Thus, one can define the point source moment tensor as

$$M_{kl} = \iint_\Sigma [u_i(\xi,\tau)]\, \hat{n}_j(\xi) C_{ijkl}(\xi)\; d\Sigma. \tag{2.15}$$

One can presume that the Σ is a planar surface and n̂ can be withdrawn from the integral because n̂ represents the normal of a fault, so it never changes for different part of the surface. Additionally, $C_{ijkl}(\xi)$ can be assumed as fixed on the fault plane. When these assumptions are applied to the equation 2.15, we can expressed the equation as

$$M_{kl} = \hat{n}_j C_{ijkl} \iint_\Sigma [u_i]\; d\Sigma. \tag{2.16}$$

If we consider the slip function as a constant, the average of slip can be taken on the fault surface as $[\bar{u}_i] := \frac{\iint_\Sigma [u_i(\xi,\tau)] d\Sigma}{A}$, where $A = \iint_\Sigma d\Sigma$ equals to fault surface area. With these considerations, moment tensor of a point source can be simplified as

$$M_{kl} = [\bar{u}_i]\, n_j C_{ijkl}, \tag{2.17}$$

where $n = A\hat{n}$ represents the fault normal vector whose magnitude equals to fault plane area and $\bar{u}_i$ becomes constant as mentioned above. Therefore the equation 2.12

with the displacement at the measurement point and time $u_n(\mathbf{x}, t)$ can be written as

$$u_n(\mathbf{x}, t) = M_{kl} * G_{nk,l}(\mathbf{x}, t; \bar{\xi}, \tau). \tag{2.18}$$

Consequently, in equation 2.18, moment tensor is derived for the point source assumption instead of moment density tensor (equation 2.13).

2.7. Fault Plane Parameters

Fault is described as boundary in volume of rock, which can be explained as planar fracture or discontinuity. Orientation of fault can be determined on Cartesian coordinates such that strike (ϕ), dip (δ) and slip (λ) angles . Moreover, in order to explain relation between these angles and moment tensor one can express these angles by slip vector ($\mathbf{u}$) and fault normal ($\mathbf{n}$)

Strike (ϕ) is measured clockwise from north which is the direction of surface intersection of the fault, this angle can vary between $0 \leq \phi \leq 2\pi$. Dip (δ) is measured clockwise from horizontal plane, which is the slop angle of the foot-wall block, the angle δ can vary in the array $0 \leq \delta \leq \frac{\pi}{2}$. Slip ($\lambda$) is measured counterclockwise from strike and slip direction, which describes the direction of fault movement and the angle λ can vary between -$\pi \leq \lambda \leq \pi$.

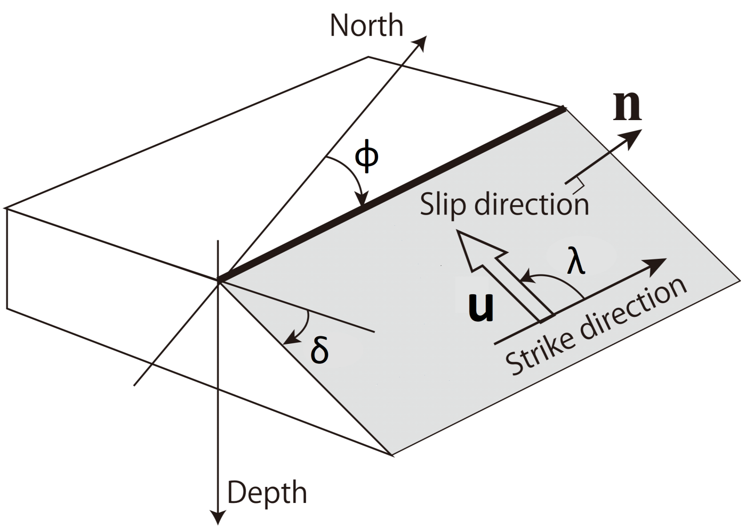

Figure 2.4. Fault Plane Expression.

In order to calculate slip vector ($\mathbf{u}$) and fault normal ($\mathbf{n}$), strike (ϕ), dip (δ) and slip (λ) should be known. This relation is calculated by [26] as

$$\begin{aligned}\mathbf{u} &= \overline{u}(\cos\lambda + \cos\Phi + \cos\delta\sin\lambda\sin\Phi)\mathbf{e}_x \\ &+ \overline{u}(\cos\lambda + \sin\Phi - \cos\delta\sin\lambda\cos\Phi)\mathbf{e}_y \\ &- \overline{u}(\sin\delta\sin\lambda)\mathbf{e}_z\end{aligned} \tag{2.19}$$

$$\mathbf{n} = -\sin\delta\sin\Phi\mathbf{e}_x + \sin\delta\cos\Phi\mathbf{e}_y - \cos\delta\mathbf{e}_z \tag{2.20}$$

2.7.1. Decomposition of the Moment Tensor

It is a well-known result that the moment tensor can uniquely be separated into two different parts, namely isotropic (ISO) and deviatoric (DEV) parts. Moreover, deviatoric part can also be expressed as a sum of two parts, double-couple (DC) and compensated linear vector dipole (CLVD). The sum of CLVD and isotropic parts is referred to non-DC components of moment tensor and it is well-known fact that tensile sources generate non-DC components. For example, explosions or seismic activities in the volcanic or geothermal areas [5][1].

Mathematically stating decomposition into isotropic and deviatoric components can uniquely be written as

$$\mathbf{M} = \mathbf{M}^{ISO} + \mathbf{M}^{DEV}. \tag{2.21}$$

However, the deviatoric part can further be decompose into DC and CLVD components. This feature leads to a non-unique decomposition. Due to its non uniquless there are various methods for the moment tensor decomposition [1], [6], [7], in a sense, these decompositions may lead to different interpretations. In this thesis the decomposition method, which is proposed by Knopof and Fitch [7],[8], is used. The ISO, DC and

CLVD decomposition can be written as

$$\mathbf{M} = \mathbf{M}^{ISO} + \mathbf{M}^{DC} + \mathbf{M}^{CLVD}, \tag{2.22}$$

where

$$\begin{aligned} \mathbf{M}^{ISO} &= \frac{1}{3} tr(\mathbf{M}) \begin{bmatrix} 1 & 0 & 0 \\ 0 & 1 & 0 \\ 0 & 0 & 1 \end{bmatrix}, \\ \mathbf{M}^{CLVD} &= |\varepsilon| M^{*}_{|max|} \begin{bmatrix} 1 & 0 & 0 \\ 0 & -2 & 0 \\ 0 & 0 & 1 \end{bmatrix}, \\ \mathbf{M}^{DC} &= (1 - 2|\varepsilon|) M^{*}_{|max|} \begin{bmatrix} -1 & 0 & 0 \\ 0 & 0 & 0 \\ 0 & 0 & 1 \end{bmatrix}. \end{aligned} \tag{2.23}$$

In equation 2.23, $\mathbf{M^*}$ denotes the deviatoric moment where $M^{*}_{|max|}$ denotes the maximum eigenvalue of $\mathbf{M^*}$ in an absolute sense and and $M^{*}_{|min|}$ denotes the minumum eigenvalue of $\mathbf{M^*}$ in an absolute sense respectively. Additionally, the value ε, which is equal to $\varepsilon = -\frac{M^{*}_{|min|}}{M^{*}_{|max|}}$, defines the size of CLVD with respect to DC (Sipkin, 1986, [5]; Kuge and Lay, 1994 [9]; Julian et al., 1998 [10], Vavryčuk, 2001, [11]).

3. DATA AND METHOD

3.1. Moment and Source Tensors Expressed in Kelvin Notation

In order to identify the moment tensor structure for the different type of sources such as shear and tensile, elasticity tensor should be considered as a linear transformation in $\mathbb{R}^6$ between the moment tensors space and source tensors space. Secondly, while using Kelvin mapping one can use the capable linear algebraic manipulation tools. In order to present equation 2.17 in Kelvin notation, firstly notice that it can be expressed as

$$\begin{aligned} M_{kl} &= \frac{1}{2} C_{ijkl} \left([u_i(\xi, \tau)] \, n_j + [u_j(\xi, \tau)] \, n_i \right) \\ &= C_{ijkl} D_{ij}, \end{aligned} \tag{3.1}$$

where u_i represents the constant and average slip function instead of $\bar{u}_i$. Due to the symmetry of elasticity tensor, first equality can be written $C_{ijkl} = C_{jikl}$. The second-rank source tensor D_{ij} in the second equality is constructed by the tensor product of $[\mathbf{u}]$ and $\mathbf{n}$. (Heaton and Heaton, 1989, [12]; Vavryčuk, 2005, [13]).

$$\begin{aligned} D_{ij} &= \frac{1}{2} \left([u_i] \, n_j + [u_j] \, n_i \right), \\ &= \frac{1}{2} \begin{bmatrix} 2 [u_1] \, n_1 & [u_1] \, n_2 + [u_2] \, n_1 & [u_1] \, n_3 + [u_3] \, n_1 \\ [u_1] \, n_2 + [u_2] \, n_1 & 2 [u_2] \, n_2 & [u_2] \, n_3 + [u_3] \, n_2 \\ [u_1] \, n_3 + [u_3] \, n_1 & [u_2] \, n_3 + [u_3] \, n_2 & 2 [u_3] \, n_3 \end{bmatrix} \end{aligned} \tag{3.2}$$

In order to simplify the equation 3.2, one can write the equation by using tensor product as

$$\mathbf{D} = \frac{1}{2} \left([\mathbf{u}] \otimes \mathbf{n} + \mathbf{n} \otimes [\mathbf{u}] \right). \tag{3.3}$$

When the tensor products image space $\mathbf{a} \otimes \mathbf{b}$ is considered as a linear transformation, it becomes one dimensional and more explicit image space, which is spanned by vector $\mathbf{a}$ since $(\mathbf{a} \otimes \mathbf{b})(\mathbf{v}) = \mathbf{a}(\mathbf{b}.\mathbf{v})$. Image space of the source tensor is defined as a plane in $\mathbb{R}^3$ and it is spanned by two vectors namely slip and normal (equation 3.3).

Notice that the equation 3.2 is the closer form of the Hooke's law equation 2.3 In both equations fourth-rank elasticity tensor meets two second-rank tensors. For that reason one can use Kelvin mapping to identify the tensors in matrix form. The advantages of the Kelvin mapping is that firstly, the elastic energy is preserved by using Kelvin mapping and it also preserves the norm of three tensors. Moreover, Kelvin mapping allows us to keep advantages of the tensor algebra e.g evaluating eigenvalues of eigenvectors of the tensors. To use Kelvin notation, one should identify the norm-preserving map, which maps the space of symmetric second-rank tensor to six dimensional vectors as below

$$\begin{bmatrix} M_{11} & M_{12} & M_{13} \\ M_{12} & M_{22} & M_{23} \\ M_{13} & M_{23} & M_{33} \end{bmatrix} \rightarrow \begin{bmatrix} M_{11} \\ M_{22} \\ M_{33} \\ \sqrt{2}M_{23} \\ \sqrt{2}M_{13} \\ \sqrt{2}M_{12} \end{bmatrix}, \begin{bmatrix} D_{11} & D_{12} & D_{13} \\ D_{12} & D_{22} & D_{23} \\ D_{13} & D_{23} & D_{33} \end{bmatrix} \rightarrow \begin{bmatrix} D_{11} \\ D_{22} \\ D_{33} \\ \sqrt{2}D_{23} \\ \sqrt{2}D_{13} \\ \sqrt{2}D_{12} \end{bmatrix}. \tag{3.4}$$

While doing the mapping above, Frobenius norm is preserved. Frobenius norm is defined as the square root of the sum of the absolute squares of its entries.In this condition Frobenius norm of second-rank tensors and vectors are equal each other.

Moreover, elasticity tensor can also be expressed by using the same mapping method in the form of a 6×6 matrix without changing the Frobenius norm. (Bóna et. al. 2007, [14])

$$\mathbf{C} = \begin{bmatrix} C_{1111} & C_{1122} & C_{1133} & \sqrt{2}C_{1123} & \sqrt{2}C_{1113} & \sqrt{2}C_{1112} \\ C_{1122} & C_{2222} & C_{2233} & \sqrt{2}C_{2223} & \sqrt{2}C_{2213} & \sqrt{2}C_{2212} \\ C_{1133} & C_{1133} & C_{3333} & \sqrt{2}C_{3323} & \sqrt{2}C_{3313} & \sqrt{2}C_{3312} \\ \sqrt{2}C_{1123} & \sqrt{2}C_{2223} & \sqrt{2}C_{3323} & 2C_{2323} & 2C_{2313} & 2C_{2312} \\ \sqrt{2}C_{1113} & \sqrt{2}C_{2213} & \sqrt{2}C_{3313} & 2C_{2313} & 2C_{1313} & 2C_{1312} \\ \sqrt{2}C_{1112} & \sqrt{2}C_{2212} & \sqrt{2}C_{3312} & 2C_{2312} & 2C_{1312} & 2C_{1212} \end{bmatrix}. \tag{3.5}$$

Notice that, if we divide above matrix into four equal parts geometrically, we can see the multiplier $\sqrt{2}$ to the elements of right-top and left-bottom parts and the multiplier 2 to the elements of right-bottom parts. Because of that in equation 3.5 elements of right-top of the matrix appears twice e.g. $C_{1123} = C_{1132}$, although the entries in the right-bottom corner appears four-times e.g. $C_{2313} = C_{2331} = C_{3213} = C_{3231}$ and the elements in the left-top appears only once. Moreover, in order to represent the tensor in the form of symmetric matrix, symmetry of elasticity tensor can be used $C_{ijkl} = C_{klij}$.

After all of this, one can represent the equation 3.2 as

$$\mathbf{m} = \mathbf{C}\mathbf{d},$$

or in componentwise

$$\begin{bmatrix} m_1 \\ m_2 \\ m_3 \\ \sqrt{2}m_4 \\ \sqrt{2}m_5 \\ \sqrt{2}m_6 \end{bmatrix} = \begin{bmatrix} C_{11} & C_{12} & C_{13} & \sqrt{2}C_{14} & \sqrt{2}C_{15} & \sqrt{2}C_{16} \\ C_{12} & C_{22} & C_{23} & \sqrt{2}C_{24} & \sqrt{2}C_{25} & \sqrt{2}C_{26} \\ C_{13} & C_{23} & C_{33} & \sqrt{2}C_{34} & \sqrt{2}C_{35} & \sqrt{2}C_{36} \\ \sqrt{2}C_{14} & \sqrt{2}C_{24} & \sqrt{2}C_{34} & 2C_{44} & 2C_{45} & 2C_{46} \\ \sqrt{2}C_{15} & \sqrt{2}C_{25} & \sqrt{2}C_{35} & 2C_{45} & 2C_{55} & 2C_{56} \\ \sqrt{2}C_{16} & \sqrt{2}C_{26} & \sqrt{2}C_{36} & 2C_{46} & 2C_{56} & 2C_{66} \end{bmatrix} \begin{bmatrix} d_1 \\ d_2 \\ d_3 \\ \sqrt{2}d_4 \\ \sqrt{2}d_5 \\ \sqrt{2}d_6 \end{bmatrix} \tag{3.6}$$

. For **m** and **d** tensors in the equation 3.6 following replacements is used,

$$(1,1) \rightarrow 1, (2,2) \rightarrow 2, (3,3) \rightarrow 3,$$
$$(2,3) \rightarrow 4, (1,3) \rightarrow 5, (1,2) \rightarrow 6.$$

Because of norm preserving feature of Kelvin notation elasticity matrix can be considered as a linear transformation in $\mathbb{R}^6$. While using Kelvin notation, we take advantage of linear algebra which is used broadly in this thesis.

3.2. Tensile Source in Isotropic Focal Region

The tensile source theory depends on the case that when the slip and the normal of the fault are not perpendicular to each other i.e. $[\mathbf{u}] . \mathbf{n} \neq 0$ (Figure 3.1).

Moreover, to simplify the moment tensor representation source area has been chosen isotropic, so the form of the elasticity matrix is also modified by considering

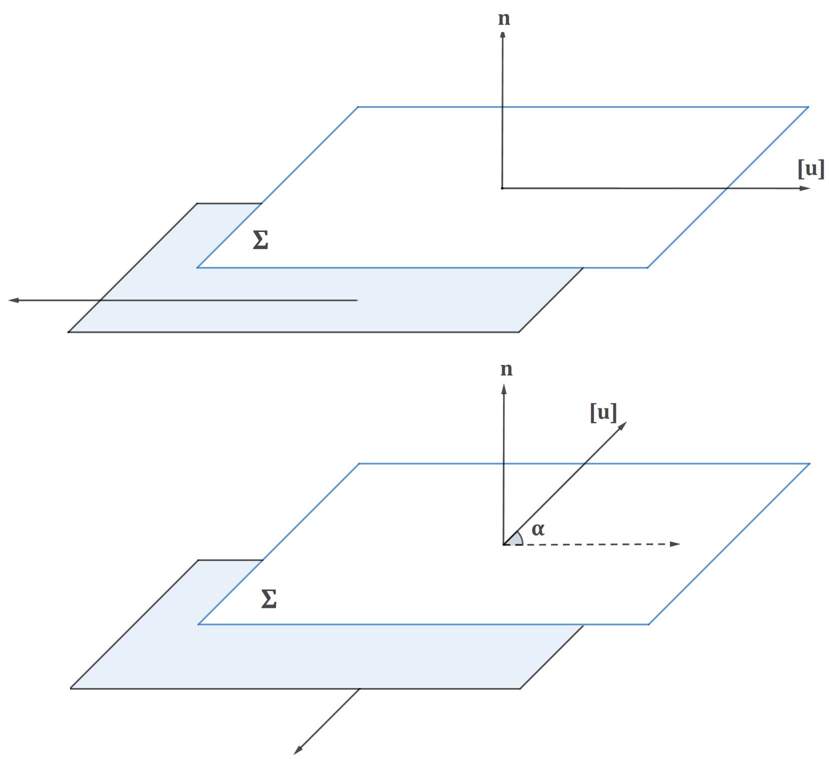

Figure 3.1. A model for the shear (above) and tensile (below), Σ represents the fault plane, $\mathbf{n}$ denotes the fault normal, $[\mathbf{u}]$ is the slip and α is the angle between slip and fault plane.

isotropic medium in Kelvin notation as

$$\mathbf{C} = \begin{bmatrix} \lambda+2\mu & \lambda & \lambda & 0 & 0 & 0 \\ \lambda & \lambda+2\mu & \lambda & 0 & 0 & 0 \\ \lambda & \lambda & \lambda+2\mu & 0 & 0 & 0 \\ 0 & 0 & 0 & 2\mu & 0 & 0 \\ 0 & 0 & 0 & 0 & 2\mu & 0 \\ 0 & 0 & 0 & 0 & 0 & 2\mu \end{bmatrix}, \tag{3.7}$$

where λ and μ represent the Lamé parameters, for that reason only two eigenspaces of isotropic elasticity tensor can be mentioned. This statement is described by Bóna et.al. (2007), [14]:

$$\mathbf{\Sigma^1} = <(1,1,1,0,0,0)>; \quad \lambda_1^C = 3\lambda + 2\mu, \tag{3.8}$$

$$\mathbf{\Sigma^2} = \{\sigma \in \mathbb{R}^6 — \sigma_1 + \sigma_2 + \sigma_3 = 0\}; \quad \lambda_2^C = 2\mu, \tag{3.9}$$

where λ_1^C and λ_2^C is the eigenvalues of the tensor in equation .

The tensile source tensor, which is in equation 3.3, differs from the shear source in that it has both isotropic and deviatoric parts ($\mathbf{d} = \mathbf{d}^{iso} + \mathbf{d}^{dev}$). Moreover, $\mathbf{d}^{iso}$ and $\mathbf{d}^{dev}$ parts of tensile source tensor depend on the different eigenspaces of the elasticity tensor. In short, $\mathbf{d}^{iso} \in \mathbf{\Sigma^1}$ and $\mathbf{d}^{dev} \in \mathbf{\Sigma^2}$ where eigenspaces are shown in equations 3.8 and 3.9. Moreover, since $(\mathbf{\Sigma^1}.\mathbf{d})\,\mathbf{\Sigma^1} = \mathbf{d}^{iso}$ Then the moment tensor can be obtained by the action of $\mathbf{C}$ onto $\mathbf{d}$, namely

$$\begin{aligned}
\mathbf{m} &= \mathbf{C}\mathbf{d} \\
&= \mathbf{C}\left(\mathbf{d}^{iso} + \mathbf{d}^{dev}\right) \\
&= \mathbf{C}\mathbf{d}^{iso} + \mathbf{C}\mathbf{d}^{dev} \\
&= \lambda_1^C \mathbf{d}^{iso} + \lambda_2^C \mathbf{d}^{dev}.
\end{aligned} \tag{3.10}$$

The moment tensor form with respect to the source tensor can be expressed equally as

$$\mathbf{M} = \lambda_1^C \mathbf{D}^{iso} + \lambda_2^C \mathbf{D}^{dev}, \tag{3.11}$$

where λ_1^C and λ_2^C are the eigenvalues of the isotropic elasticity tensor agree with the eigenspaces $\mathbf{\Sigma^1}$ and $\mathbf{\Sigma^2}$ specified in the equations 3.8 and 3.9.

The eigenvalues of the moment tensor can be acquired by utilizing the eigenvalues of the isotropic and deviatoric parts of the source tensor from equation 3.11. The statements of the eigenvalues of the moment tensor and the source tensor are shown in table 3.1. This table 3.1 also shows that in order to find the eigenvalues of the moment tensor, one can add the eigenvalues of the isotropic and deviatoric parts of the source

Table 3.1. The eigenvalues and eigenvectors in sequence of the source tensor, deviatoric and isotropic parts of the source and lastly moment tensor are expressed.

Name of the Tensor	Eigenvalues	Eigenvectors
Source Tensor $\mathbf{D}$	$\frac{1}{2}\left([\mathbf{u}]\cdot\mathbf{n}+AD\right)$	$[\hat{\mathbf{u}}]+\hat{\mathbf{n}}$
	$\frac{1}{2}\left([\mathbf{u}]\cdot\mathbf{n}-AD\right)$	$[\hat{\mathbf{u}}]-\hat{\mathbf{n}}$
	0	$[\hat{\mathbf{u}}]\times\hat{\mathbf{n}}$
$\mathbf{D}^{dev}$	$\frac{1}{2}\left([\mathbf{u}]\cdot\mathbf{n}+AD\right)-\frac{[\mathbf{u}]\cdot\mathbf{n}}{3}$	$[\hat{\mathbf{u}}]+\hat{\mathbf{n}}$
	$\frac{1}{2}\left([\mathbf{u}]\cdot\mathbf{n}-AD\right)-\frac{[\mathbf{u}]\cdot\mathbf{n}}{3}$	$[\hat{\mathbf{u}}]-\hat{\mathbf{n}}$
	$-\frac{[\mathbf{u}]\cdot\mathbf{n}}{3}$	$[\hat{\mathbf{u}}]\times\hat{\mathbf{n}}$
$\mathbf{D}^{iso}$	$\frac{[\mathbf{u}]\cdot\mathbf{n}}{3}$	Any
	$\frac{[\mathbf{u}]\cdot\mathbf{n}}{3}$	vector
	$\frac{[\mathbf{u}]\cdot\mathbf{n}}{3}$	in R^3
Moment Tensor $\mathbf{M}$	$\lambda_1^M=\frac{[\mathbf{u}]\cdot\mathbf{n}}{3}(\lambda_1^C+\frac{\lambda_2^C}{2})+\frac{\lambda_2^C}{2}AD$	$[\hat{\mathbf{u}}]+\hat{\mathbf{n}}$
	$\lambda_2^M=\frac{[\mathbf{u}]\cdot\mathbf{n}}{3}(\lambda_1^C+\frac{\lambda_2^C}{2})-\frac{\lambda_2^C}{2}AD$	$[\hat{\mathbf{u}}]-\hat{\mathbf{n}}$
	$\lambda_3^M=\frac{[\mathbf{u}]\cdot\mathbf{n}}{3}\left(\lambda_1^C-\lambda_2^C\right)$	$[\hat{\mathbf{u}}]\times\hat{\mathbf{n}}$

tensor that are multiplied by the relating eigenvalues of the elasticity tensors. This relation also expressed in equation 3.11.

3.3. Parametrization of Potency Tensor

Seismic sources can be determined by using the seismic potency tensor P_{ij}. The reason of introducing potency tensor is that it represents the source whereas moment tensor depends on the elastic parameters of the focal region. In this study the source decomposition method is used. This decomposition is proposed by Zhu and Ben-Zion [15]. Instead of stress-based moment tensor, using the strain-based potency tensor can be more effective way to explain possible fault plane and slip orientations [16].

Similar to the moment tensor, potency tensor can also be decomposed into isotropic and deviatoric parts of it.

$$P_{ij} = \frac{1}{3}tr(P)\delta_{ij} + P'_{ij}, \tag{3.12}$$

where $\mathbf{P}$ represents potency and δ_{ij} represents the Kronecker delta.

Moreover, the value ζ_p, which is a dimensionless parameter in order to quantify the strength of the isotropic part, is introduced by Zhu and Ben-Zion [17],

$$\zeta_p = \sqrt{\frac{2}{3}}\frac{tr(P)}{P_0}. \tag{3.13}$$

Note that ζ_p varies from -1 for implosion to 1 for explosion, where P_0 denotes the scalar potency and it can be formulated as $P_0 = \sqrt{2P_{ij}P_{ij}}$. Additionally, from the equation 3.13 one can rewrite the equation 3.12 as

$$P_{ij} = \frac{P_0}{\sqrt{2}}(\zeta_p I_{ij} + \sqrt{1-\zeta_p^2}D_{ij}), \tag{3.14}$$

where I_{ij} is the normalized isotropic tensor $I_{ij} = \frac{1}{\sqrt{3}}\delta_{ij}$ and D_{ij} and the value D_{ij} is the normalized deviatoric part of source tensor which is also satisfying

$$\begin{aligned} D_{ii} &= 0, \\ D_{ij} &= 1. \end{aligned} \tag{3.15}$$

Secondly, D_{ij} is decomposed to its CLVD and DC components. The CLVD has a dipole in its symmetry axis compensated by two unit dipoles in the orthogonal directions (Knopoff Randall 1970, [7]). In a sense λ_1,λ_2 and λ_3 are the eigenvalues corresponding the eigenvetors of T-axis ($\hat{T}$), null-axis ($\hat{N}$) and P-axis ($\hat{P}$) respectively. Those dimensionless eigenvalues also satisfy the three conditions, firstly $\lambda_1 \geq \lambda_2 \geq \lambda_3$, secondly $\lambda_1+\lambda_2+\lambda_3 = 0$ and thirdly $\lambda_1^2+\lambda_2^2+\lambda_3^2 = 1$. With the help of these conditions we get,

$$max(\lambda_2) = min(\lambda_1) = \frac{1}{\sqrt{6}},$$
$$min(\lambda_1) = max(\lambda_3) = \frac{1}{\sqrt{6}}. \tag{3.16}$$

If $\lambda_2 = 0$, the deviatoric tensor D_{ij} becomes pure DC. Due to the fact that CLVD symmetry axis can be adjust with all of the principal axes (e.g. Hudson et al. 1989 [18]; Jost Herrmann 1989, [6]). In this case, the CLVD symmetry axis has aligned with null-axiss (e.g. Chapman Leaney 2012, [19]).

$$\begin{aligned} D_{ij} &= \lambda_1 T_i T_j + \lambda_2 N_i N_j + \lambda_3 P_i P_j, \\ &= \frac{\lambda_1 - \lambda_3}{\sqrt{2}} D_{ij}^{DC} + \sqrt{\frac{3}{2}} \lambda_2 D_{ij}^{CLVD}, \end{aligned} \tag{3.17}$$

where

$$D_{ij}^{DC} = \frac{1}{\sqrt{2}}(T_i T_j - P_i P_j), \tag{3.18}$$
$$D_{ij}^{CLVD} = \frac{1}{\sqrt{6}}(2N_i N_j - T_i T_j - P_i P_j). \tag{3.19}$$

For the equation below, D_{ij}^{DC} and D_{ij}^{CLVD} are the normalized DC and CLVD tensors. The above decomposition has the convenient feature that the DC and CLVD basic sources are orthogonal, in other words, $D_{ij}^{DC} D_{ij}^{CLVD} = 0$. The dimensionless parameter χ_p can specify the strength of CLVD as

$$\chi_p = \sqrt{\frac{3}{2}} \lambda_2. \tag{3.20}$$

From the equation 3.16 we can get $0.5 \geq \chi_p \geq -0.5$ (Bailey et al. (2009), [20] and Julian et al. (1998), [10]) By using equation 3.15 and 3.20, equation 3.17 can be written in the form of

$$D_{ij} = \sqrt{1 - \chi_p^2} D_{ij}^{DC} + D_{ij}^{CLVD}. \tag{3.21}$$

In order to show general potency tensor as below, equation 3.21 is inserted into equation 3.14,

$$P_{ij} = \frac{P_0}{\sqrt{2}}(\zeta_p I_{ij} + \sqrt{1-\zeta_p^2}(\sqrt{1-\chi_p^2}D_{ij}^{DC} + D_{ij}^{CLVD})). \tag{3.22}$$

It can be seen, six independent values have an importance of potency tensor specification, namely: three amplitude factors P_0, ζ_p, χ_p and three angles of the principal axes of the deviatoric tensor (fault-based coordinate system with strike ϕ_p, dip δ_p and slip λ_p angles on the fault (Aki & Richards 2002, [21]).

3.4. Parametrization of Moment Tensor

General seismic moment tensor can be expressed by using same procedures,

$$M_{ij} = \sqrt{2}M_0(\zeta I_{ij} + \sqrt{1-\zeta^2}D'_{ij}), \tag{3.23}$$

where M_0 is the scalar moment described as

$$M_0 = \sqrt{\frac{M_{ij}M_{ij}}{2}} \tag{3.24}$$

and here ζ, which is a dimensionless parameter quantifying the strength of the isotropic moment, can be expressed as

$$\zeta = \frac{tr(\mathbf{M})}{\sqrt{6}M_0} \tag{3.25}$$

with the condition $1 \geq \zeta \geq -1$. In equation 3.23, the normalized deviatoric moment tensor D'_{ij} is actually represented in the same form with the D_{ij} in the equation 3.21. However, the vaule D'_{ij} uses its own eigenvalues and principal axes. Similar to the potency tensor, general moment tensor can also be explained by using six independent parameter: M_0, ζ, χ, ϕ, δ and λ. The moment tensor and potency tensor are linearly related each other through the c_{ijkl} (fourth-order elastic moduli tensor) (e.g.Ben-Zion

2013, [15]),

$$M_{ij} = c_{ijkl}P_{kl}. \tag{3.26}$$

For an isotropic elastic medium,

$$M_{ij} = (\lambda + \frac{2}{3}\mu)P_{kk}\delta_{ij} + 2\mu P_{ij}^{'} \tag{3.27}$$

where λ and μ are the Lame parameterss. By using equation 3.14 it becomes

$$M_{ij} = \sqrt{2}\mu P_0(\eta\zeta I_{ij} + \sqrt{1-\zeta^2}D_{ij}), \tag{3.28}$$

where $\eta = \frac{1+\nu}{1-2\nu}$ and ν represents the Poisson's ratio. By comparing equation 3.23 and 3.28, it can be noticed that $D_{ij}^{'} = D_{ij}$ for the isotropic elasticity. This relation explains that the CLVD variables and source orientation angles for the moment and potency tensors are the same for the isotropic medium ($\chi = \chi_p, \phi = \phi_p, \delta = \delta_p, \lambda = \lambda_p$) but isotropic parameters ζ for the moment tensor and ζ_p for the potency tensor are related as

$$\zeta = \frac{\eta\zeta_p}{\sqrt{1-(1-\eta^2)\zeta_p}}. \tag{3.29}$$

Moreover, scalar moment (M_0) and scalar potency (P_0) are also related as

$$M_0 = \mu P_0\sqrt{1-(1-\eta^2)\zeta_p} \tag{3.30}$$

Assume that there is no volumetric change in the source ($\zeta_p = 0$) equation 3.30 becomes commonly-used relationship, $M_0 = \mu P_0$ (Zhu and Ben-Zion [17]).

3.5. Moment Tensor Inversion

3.5.1. Theory of Moment Tensor Inversion

In order to find source parameters, moment tensor of seismic sources are inverted. Seismograms depend on fault parameters. Those parameters can be explained as trigonometric functions of the fault strike, dip, and slip angles. Since seismograms are linear function of entries of the moment tensor, the inverse problem is linear too. To make the inversion, moment tensor can be represented as a vector $\mathbf{m}$, which contains the six parameters of the moment tensor. Although there are nine components of a tensor, due to symmetry of a tensor only six components are independent, [22]. Then seismogram $\mathbf{u}$ at the i^{th} station can be defined as

$$u_i(t) = \sum_{j=1}^{6} G_{ij}(t) m_j, \tag{3.31}$$

where $u_i(t)$ is the seismogram in time domain, $G_{ij}(t)$ represents the Green's function in time domain which is related to the earth structure along the way from the source to station and $\mathbf{m}$ represents the moment tensor components. Due to the fact that we have more than one seismograms, we can define equation 3.31 as vector-matrix equation

$$\mathbf{u} = \mathbf{G}\mathbf{m}. \tag{3.32}$$

For the equation below, $\mathbf{u}$ is a vector composed of the seismograms at n number of stations and $\mathbf{G}$ represents the Green's function matrix. If we expand the previous equation for the n number of station case,

$$\begin{bmatrix} u_1 \\ u_2 \\ . \\ . \\ . \\ . \\ . \\ u_n \end{bmatrix} = \begin{bmatrix} G_{11} & G_{12} & G_{13} & G_{14} & G_{15} & G_{16} \\ G_{12} & G_{22} & G_{23} & G_{24} & G_{25} & G_{26} \\ . & . & . & . & . & . \\ . & . & . & . & . & . \\ . & . & . & . & . & . \\ . & . & . & . & . & . \\ . & . & . & . & . & . \\ G_{n1} & G_{n2} & G_{n3} & G_{n4} & G_{n5} & G_{n6} \end{bmatrix} \begin{bmatrix} m_1 \\ m_2 \\ m_3 \\ m_4 \\ m_5 \\ m_6 \end{bmatrix}. \tag{3.33}$$

However, this linear equation is an overdetermined system. There are n number of equations, which are more than six unknowns. Additionally, one can not invert matrix **G** because it is not a square matrix. In this condition, instead of inverting matrix **G**, closest moment tensor can be found by using observed seismograms in a least square sense [22]. In other words, generalized inverse of **G** can be used, namely

$$\mathbf{m} = (G^T G)^{-1} G^T \mathbf{u}. \tag{3.34}$$

Due to the fact that moment tensor components are represented as linear functions of the seismograms, they can be inverted in order to find the tensor components, [22].

3.5.2. Application of Moment Tensor Inversion

There are several methods of inversion of moment tensor but in this thesis gCAP (generalized cut and paste) waveform inversion method is used. The gCAP method based on the decomposition proposed by Zhu and Ben-Zion [17], [23]. This method divides three component waveforms into five windows, which are vertical and radial component Pnl; vertical and radial component Rayleigh wave; and transverse component Love waves. The advantage of breaking waveforms into different windows is that one can filter windows differently in terms of diverse frequencies in order to optimize the level of fit during the inversion [24].

The CAP method carries out a grid search over a double-couple mechanisms and this method also allows us to generate synthetic waves, which are used as data in this thesis. In order to account for errors in the Green's functions, synthetic waveforms for Pnl, Rayleigh and Love phases are also used with shifting in time property [25].

Moreover, the result of gCAP inversion includes strike, dip, rake, M_w, hypocentral depth and additionally ζ and χ parameter for possible ISO and CLVD part of source. From the zero initial values for ζ, χ and M_w grid search is performed repeatedly with given step sizes [24]. At the end of each grid search, a quadratic interpolation takes place in the vicinity of the grid point with a minimum misfit to identify the best parameter value and calculate the locally curved area to estimate the value uncertainty.

4. EXPERIMENTS AND RESULTS

In this chapter, firstly data set and the locations of seismometers are introduced. This process is approached as a case study.

Three different synthetic earthquakes are simulated for this study. These earthquakes mainly represented as moment tensors, which have different isotropic percentage and stations are located in different radius of the circles. For each cases 10 stations are located in every other 36 degrees and at different distances, namely 10,15,45,80 km (Figure 4.1). In order to avoid wrong calculation of earthquake magnitudes in the inversion stage, for each case two circles of stations are placed, which are at the different distances from the source. If stations are selected in the one circle with the same radius for the inversion, magnitudes can be calculated wrongly for the reason that gCAP inversion consider the amplitude differences of a wave in the stations with different distances when calculating the magnitude of an earthquake.

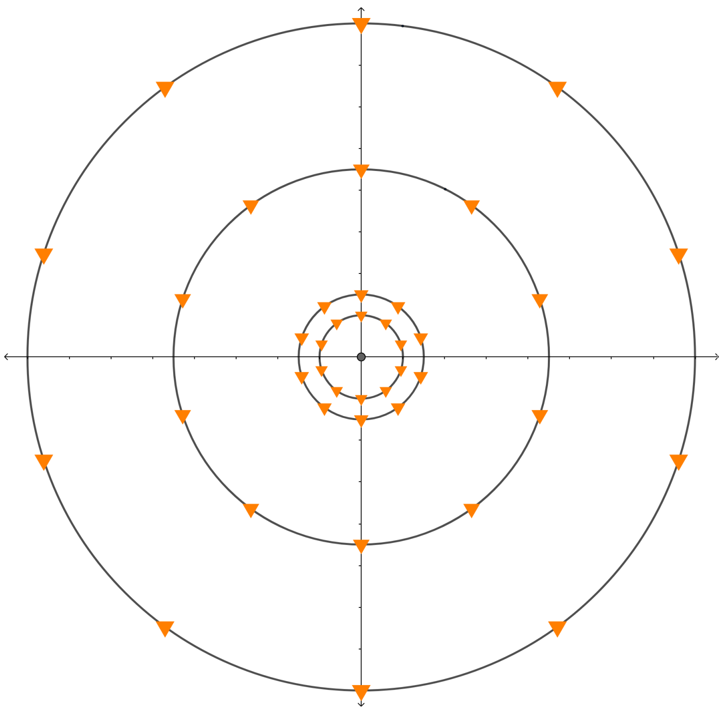

Figure 4.1. Station distribution with respect to source location. Circles are away from the source point respectively 10,15,45 and 85 km, triangles represnts the synthetic stations.

For three different moment tensors, which has different percentage of isotropy, inversions are calculated in different distances, depths. For all cases, same one layer half-space velocity model, which has 6 km/s P velocity and 3.37 km/s S velocity, is used . Velocities of P and S waves in the model are selected by considering the average velocities of P and S waves for the selected depths.

In this thesis, for each cases firstly moment tensor inversion is performed with the original percentage of isotropy, DC and CLVD and then inversions are manipulated with different values of ζ and χ in order to determine how the variance reduction is changing for wrong values of ζ. More precisely, we want to find the sensitivity of the waveforms and also inversion to the isotropic component of moment tensor, namely parameter ζ. In gCAP inversion process, one can set the ζ and χ value as a constant in the range of -1 and 1.

4.1. Case 1: Inversion of moment tensor with 2% isotropic component

For this case, our original moment tensor is

$$\mathbf{M} = \begin{bmatrix} 0.653 & 4.287 & 0.659 \\ 4.282 & 5.493 & 2.635 \\ 0.659 & 2.635 & -3.73 \end{bmatrix}, \tag{4.1}$$

which has $\zeta = 0.143$ and $\chi = -0.309$ values. This moment tensor can be decomposed as $M = 2.032\%\text{ISO} + 97.968\%\text{DEV}$ (equation 4.2). This earthquake also has the $M_0 = 6.93E+17$ Dyne-cm, $M_w = 1.16$ and other initial parameters are shown in Table 4.1.

$$\mathbf{M} = \underbrace{\begin{bmatrix} 0.806 & 0.000 & 0.000 \\ 0.000 & 0.806 & 0.000 \\ 0.000 & 0.000 & 0.806 \end{bmatrix}}_{M^{ISO}} + \underbrace{\begin{bmatrix} 1.382 & 2.933 & -0.172 \\ 2.933 & 4.124 & 3.041 \\ -0.172 & 3.041 & -5.507 \end{bmatrix}}_{M^{DC}} + \underbrace{\begin{bmatrix} -1.535 & 1.348 & 0.831 \\ 1.348 & 0.563 & -0.406 \\ 0.831 & -0.406 & 0.972 \end{bmatrix}}_{M^{CLVD}} \tag{4.2}$$

The Table 4.1 also shows the parameters as a result of inversion with the initial and original value of ζ and χ for the moment tensor.

4.1.1. Stations at 10 km and 15 km for 2% isotropy

In this case, twenty stations are placed in the two circles at 10 and 15 km far from the source point for the inversion. Table 4.1 shows the initial values of the moment tensor and its inverted results. Inversion results are obtained without imposing any parameters such as ζ and χ, which defines the percentages of ISO and CLVD.

Table 4.1. Initial values and inversion results of an earthquake parameters with 98.4 variance reduction in the stations, which are placed at circle with 10 and 15 km radius for the case 1.

Case 1.1	M_0	M_w	Strike	Dip	Rake	ISO%	DC%	CLVD%	ζ	χ
Initial	6.93E+17	1.16	343	59	-72	2.032	88.620	9.347	0.143	-0.309
Inverted	6.89E+17	1.16	346	60	-69	2.031	88.608	9.361	0.143	-0.309

As a result of inversion, variance reduction is obtained as 98.4 and parameters of the moment tensor haven't changed much (Table 4.1 and equation 4.3).

$$\mathbf{M^{inv}} = \begin{bmatrix} 0.578 & 4.278 & 0.578 \\ 4.279 & 5.393 & 2.752 \\ 0.577 & 2.752 & -3.570 \end{bmatrix} \tag{4.3}$$

Secondly, inversions are manipulated for the different isotropic percentages (different ζ values). More precisely, apart from original ζ value for the moment tensor, other possible values of ζ are imposed in the inversion in the range of -1 to 1 with the step of 0.1. Totally 21 inversions are performed for the changing ζ values.

As a result of inversions, results are shown in the Figures 4.2, 4.3, 4.4, 4.5. Figure 4.2 shows how the variance reduction changes as the isotropic percentage varies. These plots show the sensitivity of the inversion to isotropic percentage of the moment tenor. In figures 4.3, 4.4, 4.5, the changes in strike, dip and rake angles are shown according to the variation of isotropic percentages in the range of -100% and 100%.

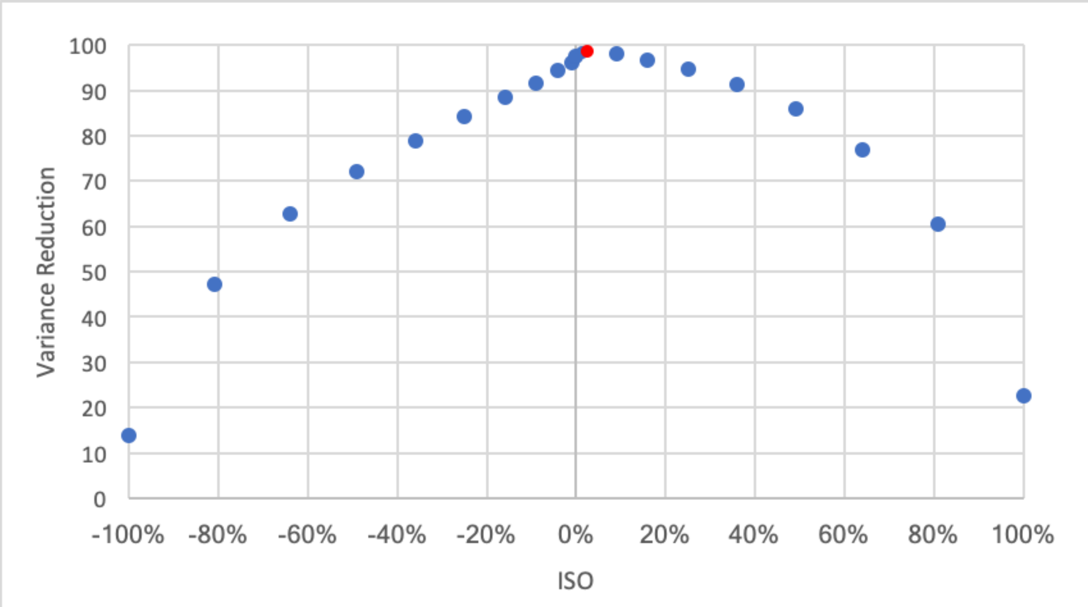

Figure 4.2. As a result of inversions, changes in the variance reduction with respect to manipulated percentages of ISO are shown. In this case, stations are placed at 10 and 15 km distances. The original moment tensor, which is expressed as red dot, has 2% isotropy. The inversions of moment tensor are done for some forced values of ISO%-percentage, which is shown in the x-axis, and the variance reduction values of the inverted moment tensors are shown in the y-axis.

Figure 4.2 reveals the fault that waveforms are not very sensitive to the isotropic component i.e even though the isotropic percentage has approximately 20% error, the synthetic waveforms fit the data by 95% (variance reduction).

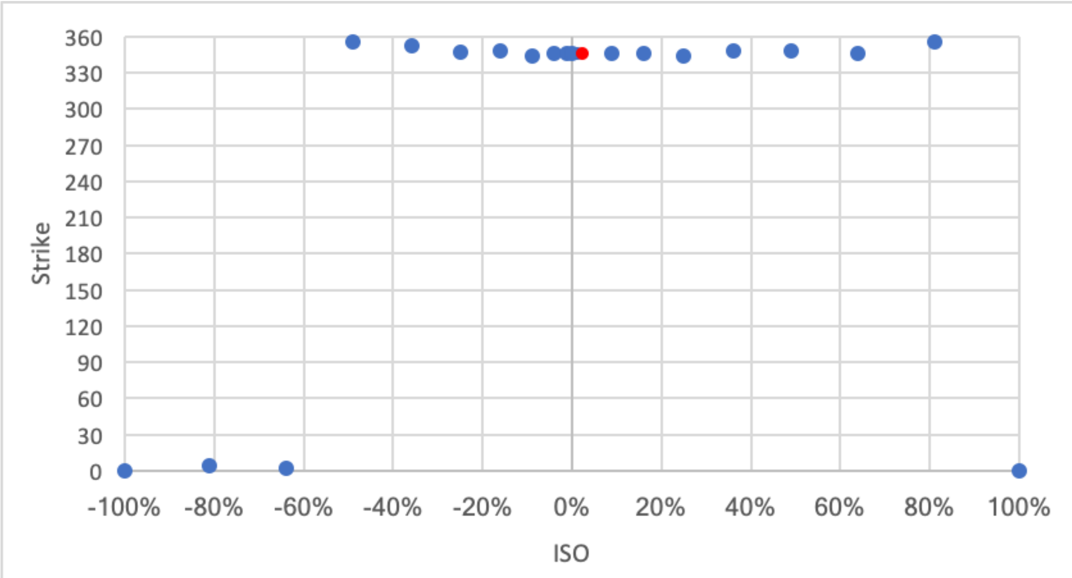

Figure 4.3. Changes in the strike angle with respect to manipulated percentages of ISO are shown as a result of inversions. In this case, stations are placed at 10 and 15 km distances and red dot in the graph shows the original moment tensor with 2% isotropy. The inversions of moment tensor are done for some forced values of ISO%-percentage, which is shown in the x-axis, and the strike angles of the inverted moment tensors are shown in the y-axis.

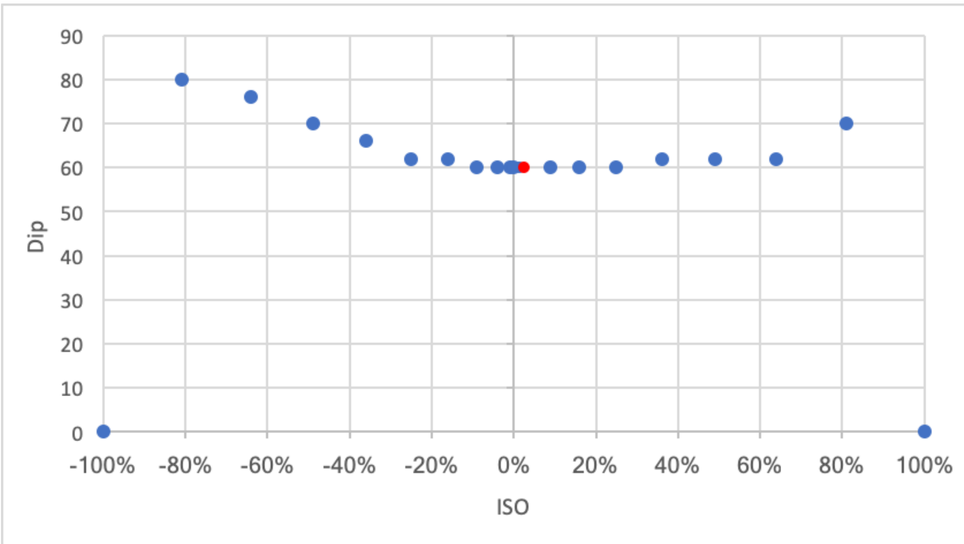

Figure 4.4. Changes in the dip angle with respect to manipulated percentages of ISO are shown as a result of inversions. In this case, stations are placed at 10 and 15 km distances and red dot in the graph shows the original moment tensor with 2% isotropy. The inversions of moment tensor are done for some forced values of ISO%-percentage, which is shown in the x-axis, and the dip angles of the inverted moment tensors are shown in the y-axis.

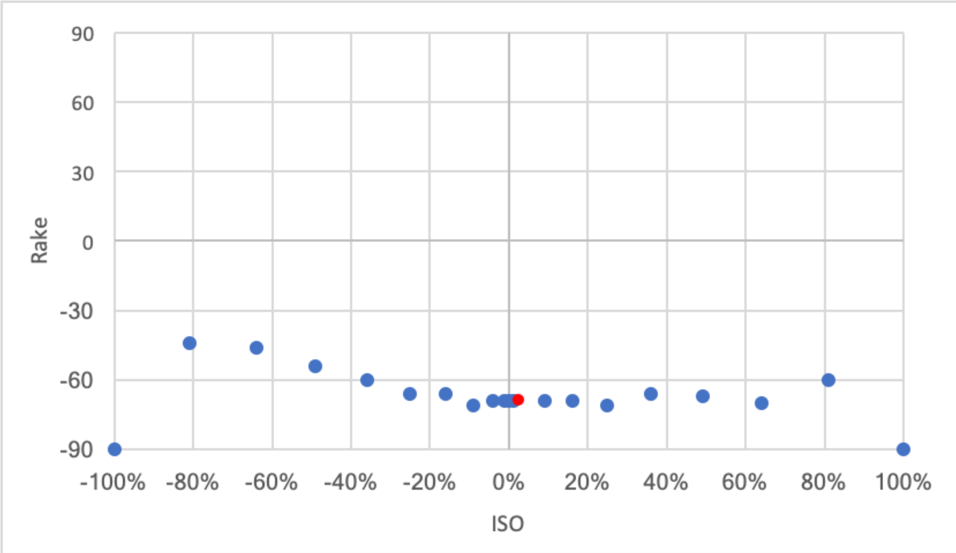

Figure 4.5. Changes in the rake angle with respect to manipulated percentages of ISO are shown as a result of inversions. In this case, stations are placed at 10 and 15 km distances and red dot in the graph shows the original moment tensor with 2% isotropy. The inversions of moment tensor are done for some forced values of ISO%-percentage, which is shown in the x-axis, and the rake angles of the inverted moment tensors are shown in the y-axis.

For figure 4.3, 4.4 and 4.5, the results are expected same. Isotropic percentage should not change the values of strike-dip-rake. In fact, strike-dip-rake are derived from the double couple component of moment tensor, not the isotropic component of moment tensor.

4.1.2. Stations at 45 km and 80 km for 2% isotropy

In this case, ten stations are placed in a circle with 45 km radius and other ten stations placed in a circle which is 80 km far from the source point. Table 4.2 shows the initial values of the moment tensor and its inverted results. Inversion results are obtained without imposing any parameters such as ζ and χ, which defines the percentages of ISO and CLVD.

Table 4.2. Initial values and inversion results of an earthquake parameters with 96.7 variance reduction in the stations, which are placed at circles with 45 and 85 km radius for the case 1.

Case 1.2	M_0	M_w	Strike	Dip	Rake	ISO%	DC%	CLVD%	ζ	χ
Initial	6.93E+17	3.16	343	59	-72	2.032	88.620	9.347	0.143	-0.309
Inverted	7.67E+17	3.19	340	56	-77	2.052	88.597	9.351	0.143	-0.309

Variance reduction is obtained as 96.7% after the inversion and other parameters of moment tensor are shown in Table 4.2 and equation 4.4.

$$\mathbf{M^{inv}} = \begin{bmatrix} 0.798 & 4.742 & 0.714 \\ 4.742 & 6.284 & 2.494 \\ 0.714 & 2.494 & -4.389 \end{bmatrix} \tag{4.4}$$

Afterwards, inversion parameters are manipulated for the different isotropic percentages (different ζ values). More precisely, apart from the original ζ value of the moment tensor, other possible values of ζ are forced in the range of -1 to 1 with the step of 0.1. Totally 21 inversions are performed for the changing ζ values.

As a result of inversions, results are shown in the Figures 4.6, 4.7, 4.8, 4.9. Figure 4.6 shows how the variance reduction changes as the isotropic percentage varies. These plots show the sensitivity of the inversion to isotropic percentage of the moment tenor. In figures 4.7, 4.8, 4.9, the changes in strike, dip and rake angles are shown according to the variation of isotropic percentages in the range of -100% and 100%.

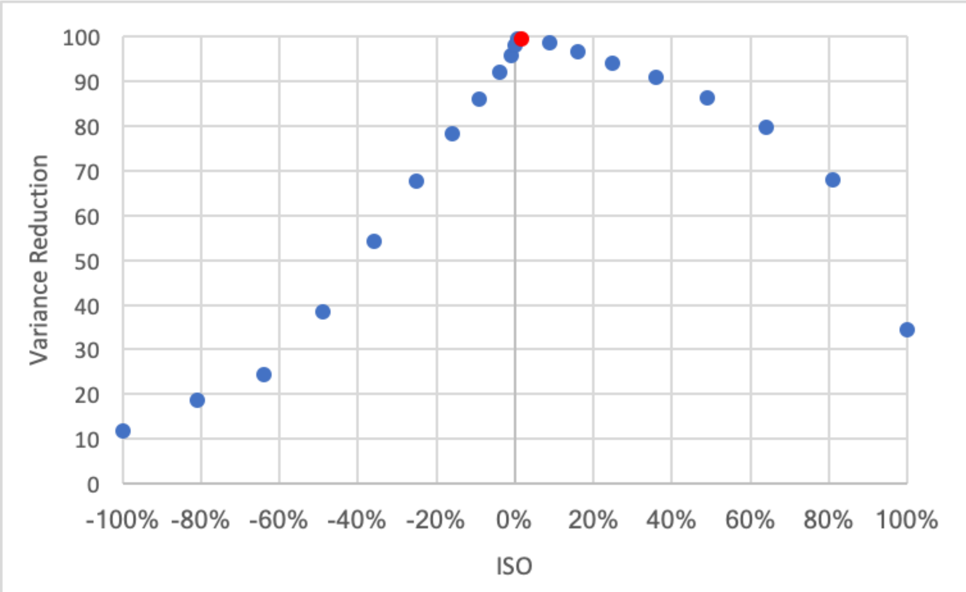

Figure 4.6. As a result of inversions, changes in the variance reduction with respect to manipulated percentages of ISO are shown. In this case, stations are placed at 45 and 80 km distances. The original moment tensor, which is expressed as red dot, has 2% isotropy. The inversions of moment tensor are done for some forced values of ISO%-percentage, which is shown in the x-axis, and the variance reduction values of the inverted moment tensors are shown in the y-axis.

Figure 4.6 reveals the fault that waveforms are not very sensitive to the isotropic component i.e even though the isotropic percentage has approximately 20% error, the synthetic waveforms fit the data by 95% (variance reduction).

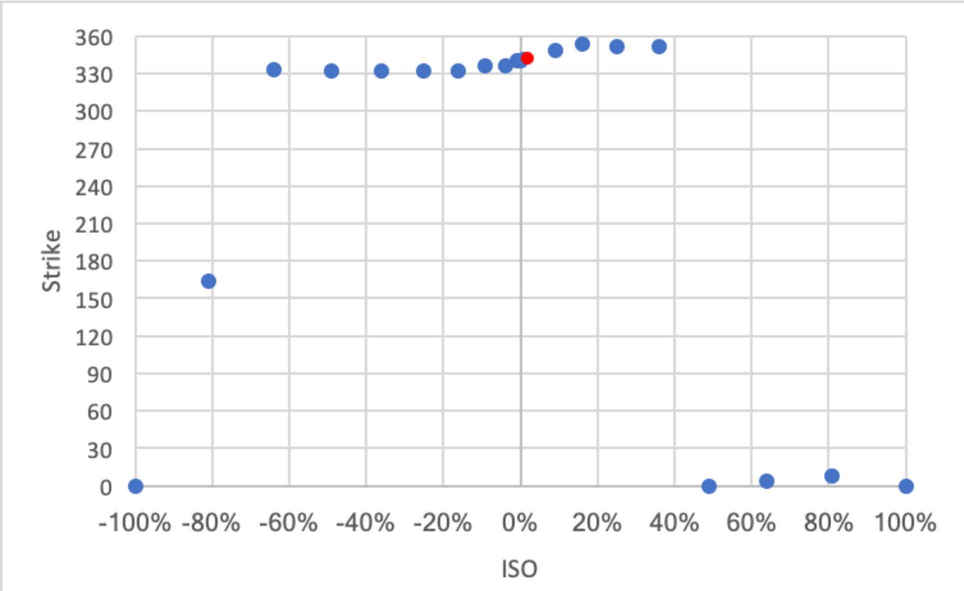

Figure 4.7. Changes in the strike angle with respect to manipulated percentages of ISO are shown as a result of inversions. In this case, stations are placed at 45 and 80 km distances and red dot in the graph shows the original moment tensor with 2% isotropy. The inversions of moment tensor are done for some forced values of ISO%-percentage, which is shown in the x-axis, and the strike angles of the inverted moment tensors are shown in the y-axis.

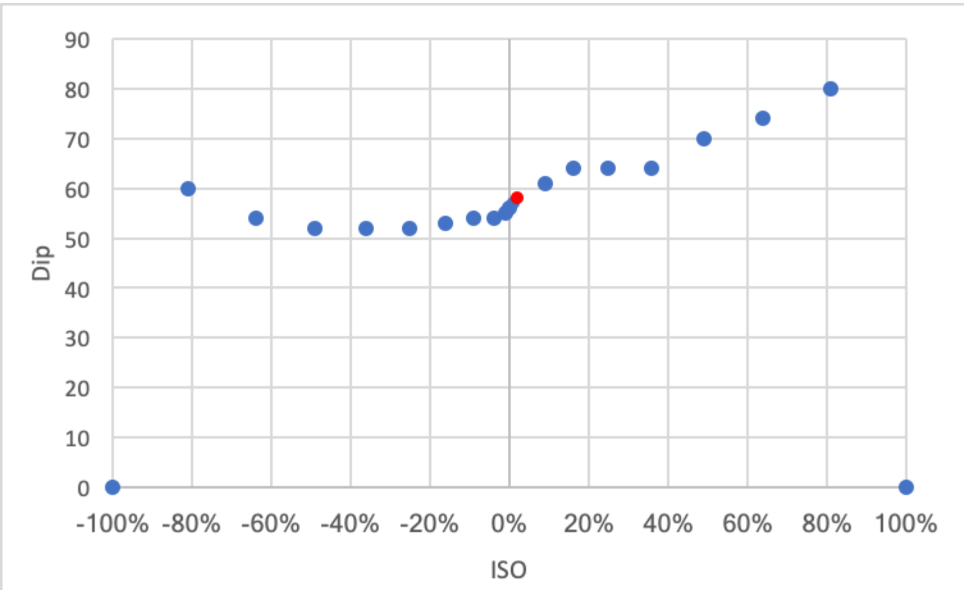

Figure 4.8. Changes in the dip angle with respect to manipulated percentages of ISO are shown as a result of inversions. In this case, stations are placed at 45 and 80 km distances and red dot in the graph shows the original moment tensor with 2% isotropy. The inversions of moment tensor are done for some forced values of ISO%-percentage, which is shown in the x-axis, and the dip angles of the inverted moment tensors are shown in the y-axis.

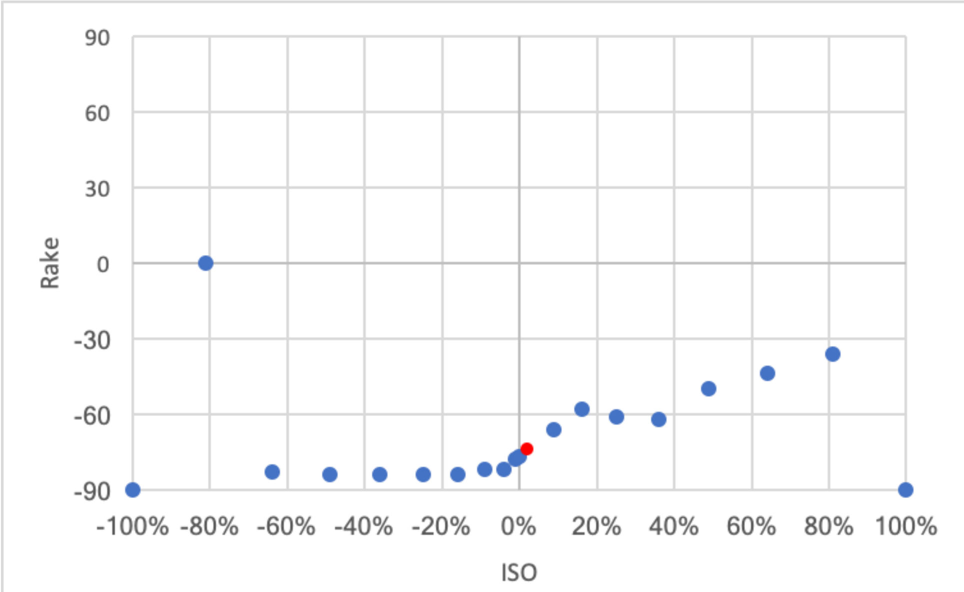

Figure 4.9. Changes in the rake angle with respect to manipulated percentages of ISO are shown as a result of inversions. In this case, stations are placed at 45 and 80 km distances and red dot in the graph shows the original moment tensor with 2% isotropy. The inversions of moment tensor are done for some forced values of ISO%-percentage, which is shown in the x-axis, and the rake angles of the inverted moment tensors are shown in the y-axis.

For figure 4.7, 4.8 and 4.9, the results are expected same. Isotropic percentage should not change the values of strike-dip-rake. In fact, strike-dip-rake are derived from the double couple component of moment tensor, not the isotropic component of moment tensor.

4.2. Case 2: Inversion of moment tensor with 5% isotropic component

For this case, our original moment tensor is

$$\mathbf{M} = \begin{bmatrix} 2.123 & 4.282 & 0.659 \\ 4.282 & 5.493 & 2.635 \\ 0.659 & 2.635 & -3.73 \end{bmatrix}. \tag{4.5}$$

In this case, moment tensor has $\zeta = 0.224$ and $\chi = -0.234$ values. This moment tensor can be decomposed as $M = 5.040\%\text{ISO} + 94.96\%\text{DEV}$ (equation 4.6). This earthquake also has the $M_0 = 7.07E+17$ Dyne-cm, $M_w = 1.17$ and other initial values are shown in Table 4.3.

$$\mathbf{M} = \underbrace{\begin{bmatrix} 1.296 & 0.000 & 0.000 \\ 0.000 & 1.296 & 0.000 \\ 0.000 & 0.000 & 1.296 \end{bmatrix}}_{M^{ISO}} + \underbrace{\begin{bmatrix} 1.863 & 3.131 & 0.110 \\ 3.131 & 3.940 & 2.956 \\ 0.110 & 2.956 & -5.802 \end{bmatrix}}_{M^{DC}} + \underbrace{\begin{bmatrix} -1.035 & 1.151 & 0.549 \\ 1.151 & 0.258 & -0.321 \\ 0.549 & -0.321 & 0.778 \end{bmatrix}}_{M^{CLVD}} \tag{4.6}$$

4.2.1. Stations at 10 km and 15 km for 5% isotropy

In this case, ten stations are placed in a circle with 10 km radius and other ten stations are placed in a circle which is 15 km far from the source point. Table 4.3 shows the initial values of the moment tensor and its inverted results. Inversion results are obtained without imposing any parameters such as ζ and χ, which defines the percentages of ISO and CLVD.

Table 4.3. Initial values and inversion results of an earthquake parameters with 96.7 variance reduction in the stations, which are placed at circles with 45 and 85 km radius for the case 2.

Case 2.1	M_0	M_w	Strike	Dip	Rake	ISO%	DC%	CLVD%	ζ	χ
Initial	7.07E+17	1.17	338	58	-74	5.040	89.759	5.201	0.224	-0.234
Inverted	7.041E+17	3.19	338	58	-74	5.024	89.789	5.187	0.224	-0.234

As a result of inversion with original ζ value, variance reduction is obtained as 98.4% and parameters of initial and inverted moment tensor are shown in Table 4.3

and equation 4.7.

$$\mathbf{M^{inv}} = \begin{bmatrix} 2.112 & 4.253 & 0.690 \\ 4.253 & 5.443 & 2.676 \\ 0.690 & 2.676 & -3.689 \end{bmatrix} \tag{4.7}$$

Secondly, inversions are manipulated for the different isotropic percentages (different ζ values). More precisely, apart from original ζ value for the moment tensor, other possible values of ζ are imposed in the inversion in the range of -1 to 1 with the step of 0.1. Totally 21 inversions are performed for the changing ζ values.

As a result of inversions, results are shown in the Figures 4.10, 4.11, 4.12, 4.13. Figure 4.10 shows how the variance reduction changes as the isotropic percentage varies. These plots show the sensitivity of the inversion to isotropic percentage of the moment tenor. In figures 4.11, 4.12, 4.13, the changes in strike, dip and rake angles are shown according to the variation of isotropic percentages in the range of -100% and 100%.

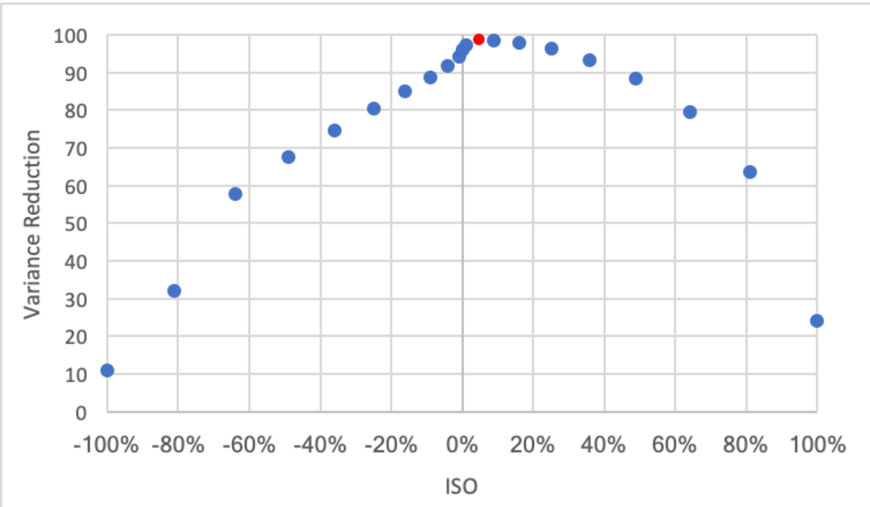

Figure 4.10. As a result of inversions, changes in the variance reduction with respect to manipulated percentages of ISO are shown. In this case, stations are placed at 10 and 15 km distances. The original moment tensor, which is expressed as red dot, has 5% isotropy. The inversions of moment tensor are done for some forced values of ISO%-percentage, which is shown in the x-axis, and the variance reduction values of the inverted moment tensors are shown in the y-axis.

Figure 4.10 reveals the fault that waveforms are not very sensitive to the isotropic component i.e even though the isotropic percentage has approximately 20% error, the synthetic waveforms fit the data by 95% (variance reduction).

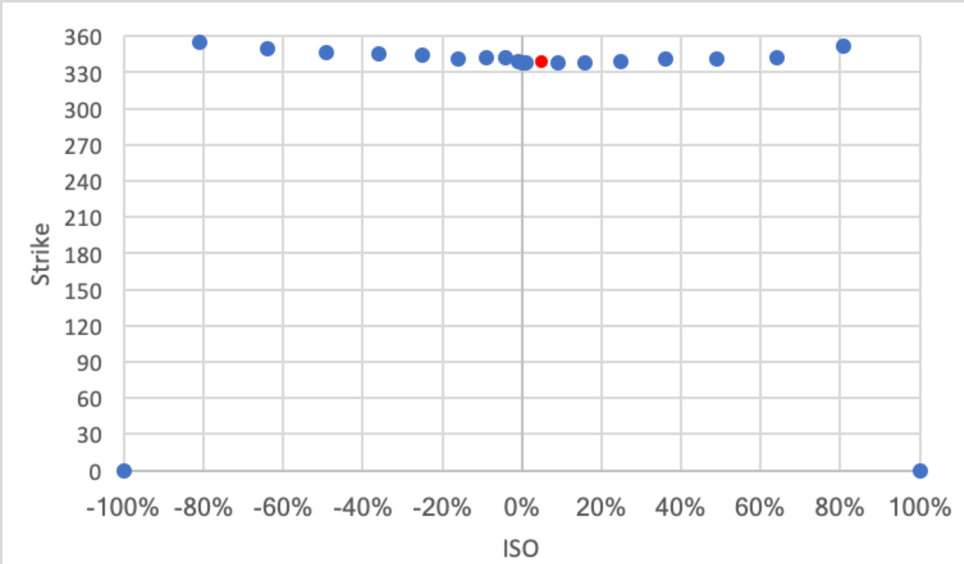

Figure 4.11. Changes in the strike angle with respect to manipulated percentages of ISO are shown as a result of inversions. In this case, stations are placed at 10 and 15 km distances and red dot in the graph shows the original moment tensor with 5% isotropy. The inversions of moment tensor are done for some forced values of ISO%-percentage, which is shown in the x-axis, and the strike angles of the inverted moment tensors are shown in the y-axis.

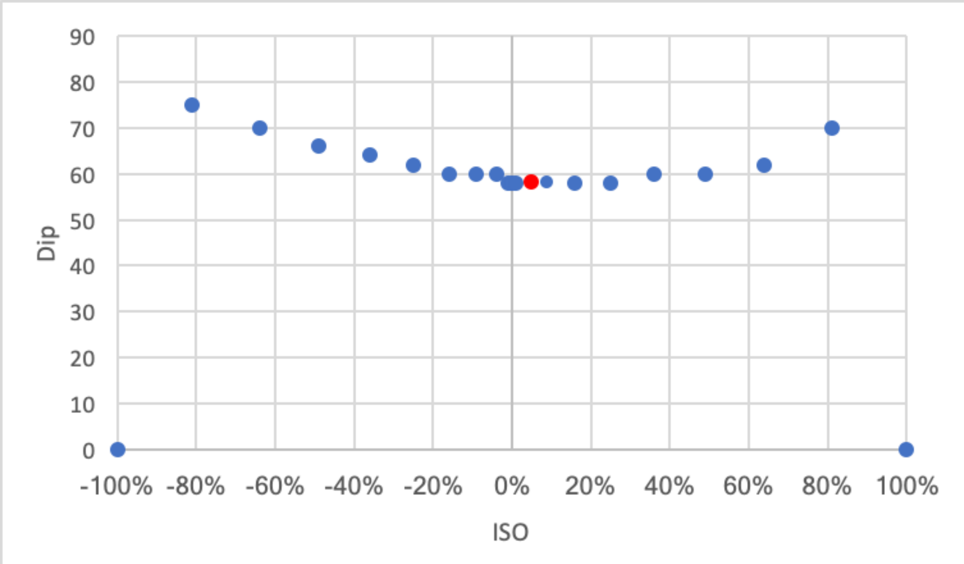

Figure 4.12. Changes in the dip angle with respect to manipulated percentages of ISO are shown as a result of inversions. In this case, stations are placed at 10 and 15 km distances and red dot in the graph shows the original moment tensor with 5% isotropy. The inversions of moment tensor are done for some forced values of ISO%-percentage, which is shown in the x-axis, and the dip angles of the inverted moment tensors are shown in the y-axis.

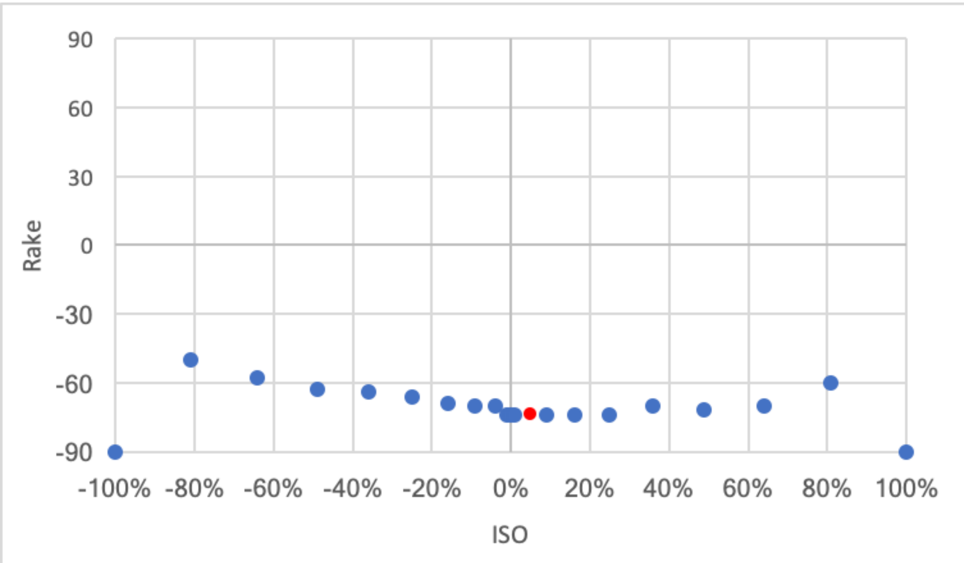

Figure 4.13. Changes in the rake angle with respect to manipulated percentages of ISO are shown as a result of inversions. In this case, stations are placed at 10 and 15 km distances and red dot in the graph shows the original moment tensor with 5% isotropy. The inversions of moment tensor are done for some forced values of ISO%-percentage, which is shown in the x-axis, and the rake angles of the inverted moment tensors are shown in the y-axis.

For figure 4.11, 4.12 and 4.13, the results are expected same. Isotropic percentage should not change the values of strike-dip-rake. In fact, strike-dip-rake are derived from the double couple component of moment tensor, not the isotropic component of moment tensor.

4.2.2. Stations at 45 km and 80 km for 5% isotropy

In this case, twenty stations are placed in the two circles at 45 and 80 km far from the source point for the inversion of full moment tensor with 5% isotropy. Table 4.4 shows the initial values of the moment tensor and its inverted results. Inversion results are obtained without imposing any parameters such as ζ and χ, which defines the percentages of ISO and CLVD.

Table 4.4. Initial values and inversion results of an earthquake parameters with 99.7 variance reduction in the stations, which are placed at circles with 45 and 85 km radius for the case 1.

Case 2.2	M_0	M_w	Strike	Dip	Rake	ISO%	DC%	CLVD%	ζ	χ
Initial	7.07E+19	3.50	338	58	-74	5.040	89.759	5.201	0.224	-0.234
Inverted	7.07E+19	3.27	338	58	-74	5.026	89.772	5.202	0.220	-0.230

Variance reduction is obtained as 99.7% after the inversion and other parametersof moment tensor are shown in Table 4.4 and equation 4.8.

$$\mathbf{M^{inv}} = \begin{bmatrix} 2.123 & 4.282 & 0.659 \\ 4.282 & 5.493 & 2.635 \\ 0.659 & 2.635 & -3.728 \end{bmatrix} \tag{4.8}$$

Afterwards, inversion parameters are manipulated for the different isotropic percentages (different ζ values). More precisely, apart from the original ζ value of the moment tensor, other possible values of ζ are forced in the range of -1 to 1 with the step of 0.1. Totally 21 inversions are performed for the changing ζ values.

As a result of inversions, results are shown in the Figures 4.14, 4.15, 4.16, 4.17.

Figure 4.14 shows how the variance reduction changes as the isotropic percentage varies. These plots show the sensitivity of the inversion to isotropic percentage of the moment tenor. In figures 4.15, 4.16, 4.17, the changes in strike, dip and rake angles are shown according to the variation of isotropic percentages in the range of -100% and 100%.

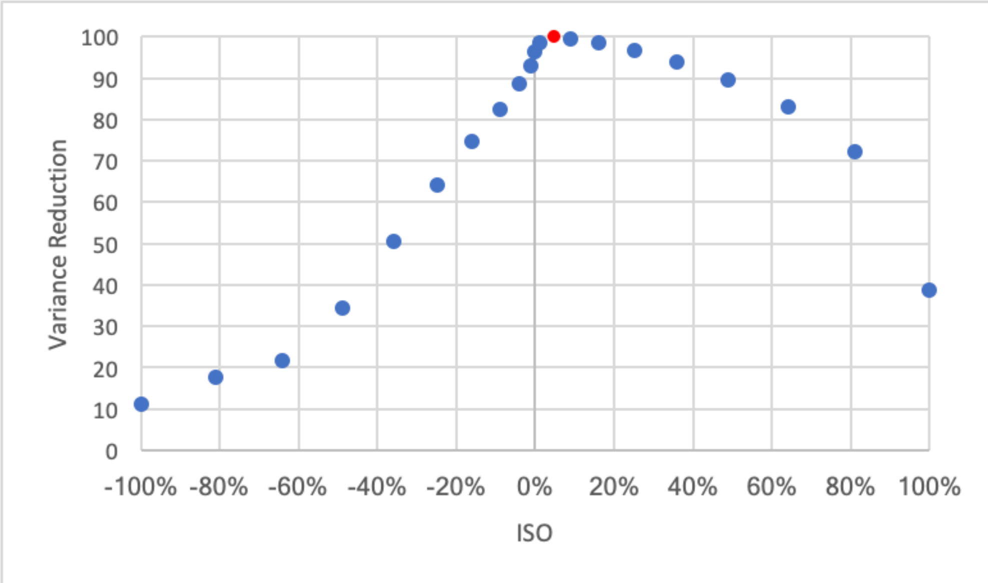

Figure 4.14. As a result of inversions, changes in the variance reduction with respect to manipulated percentages of ISO are shown. In this case, stations are placed at 45 and 80 km distances. The original moment tensor, which is expressed as red dot, has 5% isotropy. The inversions of moment tensor are done for some forced values of ISO%-percentage, which is shown in the x-axis, and the variance reduction values of the inverted moment tensors are shown in the y-axis.

Figure 4.14 reveals the fault that waveforms are not very sensitive to the isotropic component i.e even though the isotropic percentage has approximately 20% error, the synthetic waveforms fit the data by 95% (variance reduction).

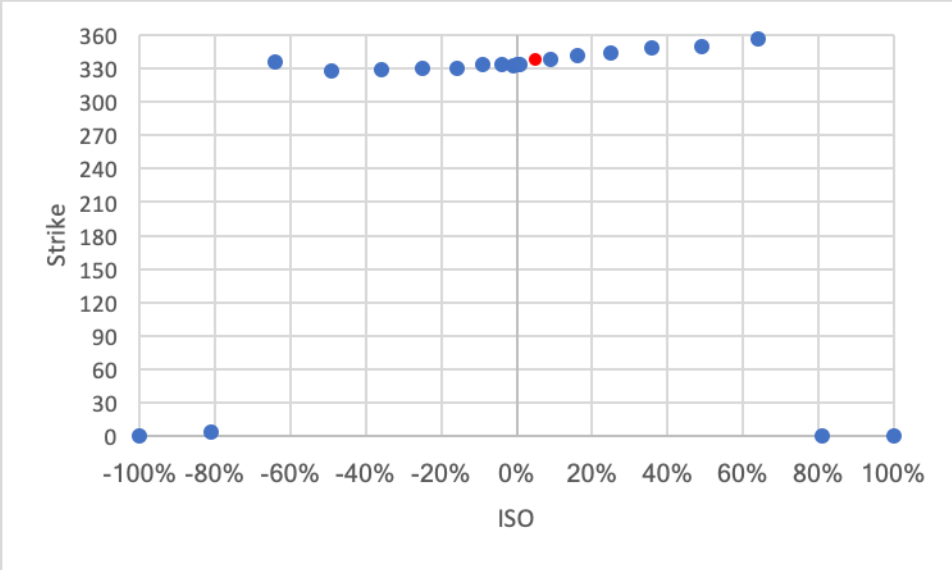

Figure 4.15. Changes in the strike angle with respect to manipulated percentages of ISO are shown as a result of inversions. In this case, stations are placed at 45 and 80m distances and red dot in the graph shows the original moment tensor with 5% isotropy. The inversions of moment tensor are done for some forced values of ISO%-percentage, which is shown in the x-axis, and the strike angles of the inverted moment tensors are shown in the y-axis.

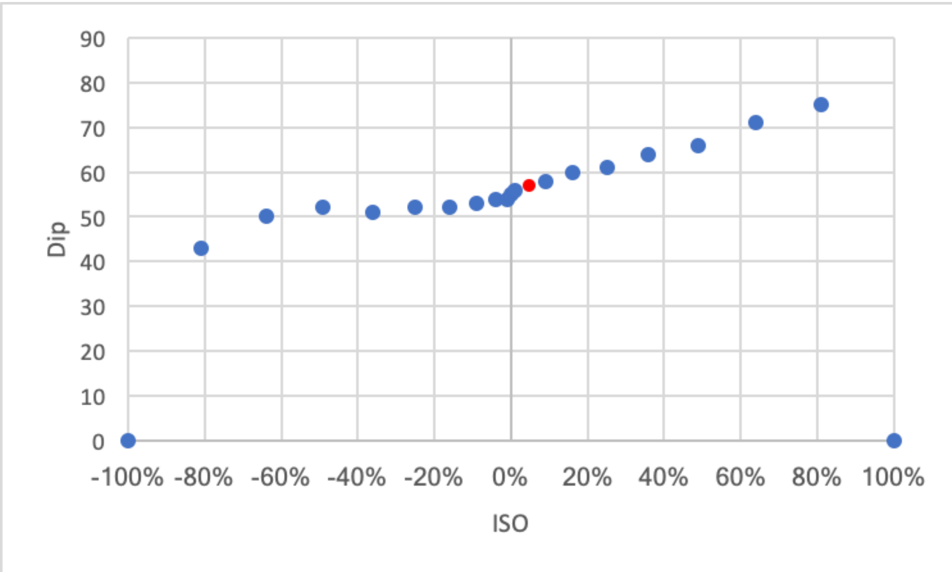

Figure 4.16. Changes in the dip angle with respect to manipulated percentages of ISO are shown as a result of inversions. In this case, stations are placed at 45 and 80 km distances and red dot in the graph shows the original moment tensor with 5% isotropy. The inversions of moment tensor are done for some forced values of ISO%-percentage, which is shown in the x-axis, and the dip angles of the inverted moment tensors are shown in the y-axis.

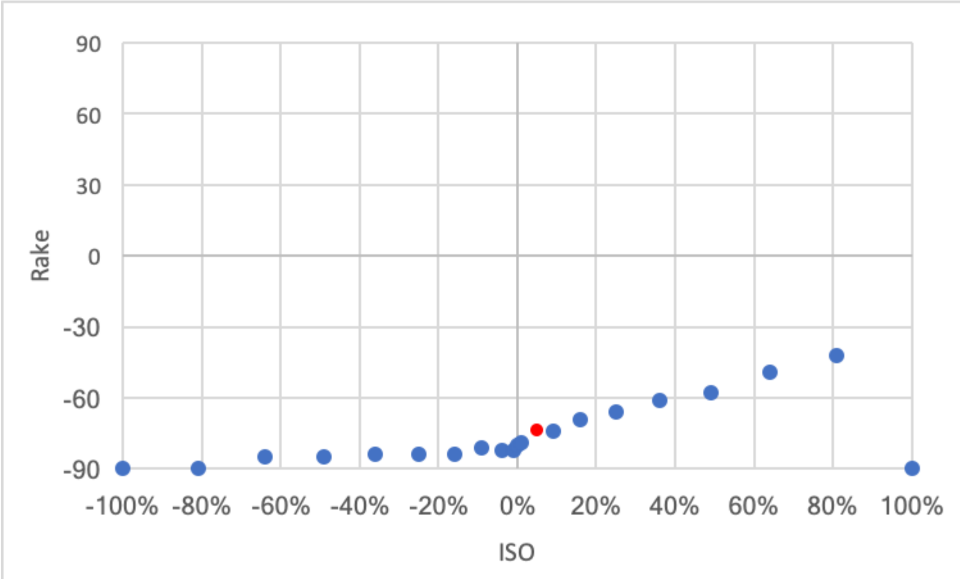

Figure 4.17. Changes in the rake angle with respect to manipulated percentages of ISO are shown as a result of inversions. In this case, stations are placed at 45 and 80 km distances and red dot in the graph shows the original moment tensor with 5% isotropy. The inversions of moment tensor are done for some forced values of ISO%-percentage, which is shown in the x-axis, and the rake angles of the inverted moment tensors are shown in the y-axis.

For figure 4.15, 4.16 and 4.17, the results are expected same. Isotropic percentage should not change the values of strike-dip-rake. In fact, strike-dip-rake are derived from the double couple component of moment tensor, not the isotropic component of moment tensor.

4.3. Case 3: Inversion of moment tensor with 14% isotropic component

For this case, our original moment tensor is

$$\mathbf{M} = \begin{bmatrix} 5.523 & 4.282 & 0.659 \\ 4.282 & 5.493 & 2.635 \\ 0.659 & 2.635 & -3.728 \end{bmatrix}, \tag{4.9}$$

which has $\zeta = 0.375$ and $\chi = -0.103$ values. This moment tensor can be decomposed as $M = 14.053\%\text{ISO} + 85.041\%\text{DEV}$ (equation 4.10). This earthquake also has the $M_0 = 7.94E + 17$ Dyne-cm, $M_w = 1.20$ and other initial parameters and inverted parameters of moment tensor are shown in Table 4.5.

$$
\mathbf{M} = \underbrace{\begin{bmatrix} 2.429 & 0.000 & 0.000 \\ 0.000 & 2.429 & 0.000 \\ 0.000 & 0.000 & 2.429 \end{bmatrix}}_{M^{ISO}} + \underbrace{\begin{bmatrix} 3.358 & 3.667 & 0.440 \\ 3.667 & 3.168 & 2.827 \\ 0.440 & 2.827 & -6.525 \end{bmatrix}}_{M^{DC}} + \underbrace{\begin{bmatrix} -0.264 & 0.615 & 0.219 \\ 0.615 & -0.104 & -0.192 \\ 0.219 & -0.192 & 0.367 \end{bmatrix}}_{M^{CLVD}} \tag{4.10}
$$

4.3.1. Stations at 10 km and 15 km for 14% isotropy

In this case, twenty stations are placed in the two circles at 10 and 15 km far from the source point for the inversion of full moment tensor with 14% isotropy. Table 4.5 shows the initial values of the moment tensor and its inverted results. Inversion results are obtained without imposing any parameters such as ζ and χ, which defines the percentages of ISO and CLVD.

Table 4.5. Initial values and inversion results of an earthquake parameters with 97.9 variance reduction in the stations, which are placed at circles with 10 and 15 km radius, for the case 3.

Case 3.1	M_0	M_w	Strike	Dip	Rake	ISO%	DC%	CLVD%	ζ	χ
Initial	7.94E+17	1.20	328	56	-74	14.053	85.041	0.906	0.375	-0.103
Inverted	7.75E+17	1.19	332	58	-69	14.033	85.071	0.906	0.379	-0.114

As a result of inversion, variance reduction is obtained as 98.4% and parameters of the moment tensor haven't changed much (Table 4.5 and equation 4.11).

$$\mathbf{M}^{\mathbf{inv}} = \begin{bmatrix} 4.990 & 4.866 & 0.798 \\ 4.866 & 5.161 & 2.573 \\ 0.798 & 2.5735 & -2.565 \end{bmatrix} \tag{4.11}$$

Secondly, inversions are manipulated for the different isotropic percentages (different ζ values). More precisely, apart from original ζ value for the moment tensor, other possible values of ζ are imposed in the inversion in the range of -1 to 1 with the step of 0.1. Totally 21 inversions are performed for the changing ζ values.

As a result of inversions, results are shown in the Figures 4.18, 4.19, 4.20, 4.21. Figure 4.18 shows how the variance reduction changes as the isotropic percentage varies. These plots show the sensitivity of the inversion to isotropic percentage of the moment tenor. In figures 4.19, 4.20, 4.21, the changes in strike, dip and rake angles are shown according to the variation of isotropic percentages in the range of -100% and 100%.

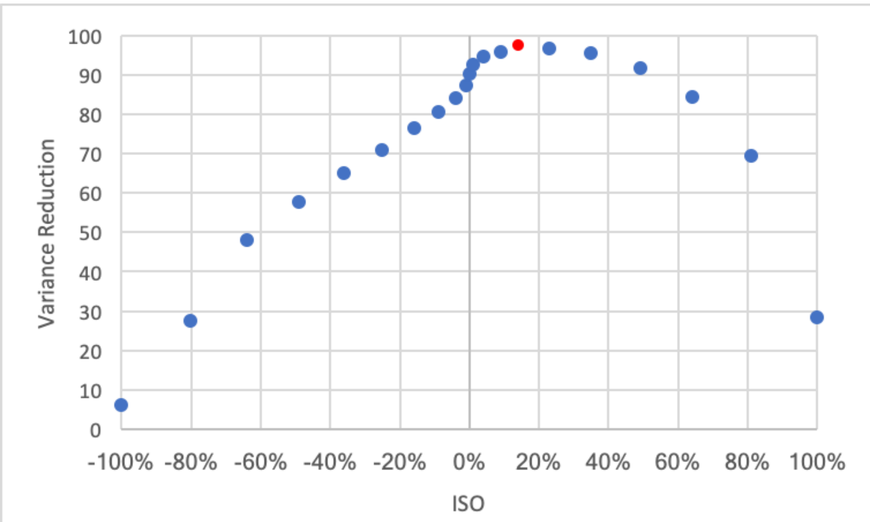

Figure 4.18. As a result of inversions, changes in the variance reduction with respect to manipulated percentages of ISO are shown. In this case, stations are placed at 10 and 15 km distances. The original moment tensor, which is expressed as red dot, has 14% isotropy. The inversions of moment tensor are done for some forced values of ISO%-percentage, which is shown in the x-axis, and the variance reduction values of the inverted moment tensors are shown in the y-axis.

Figure 4.18 reveals the fault that waveforms are not very sensitive to the isotropic component i.e even though the isotropic percentage has approximately 20% error, the synthetic waveforms fit the data by 95% (variance reduction).

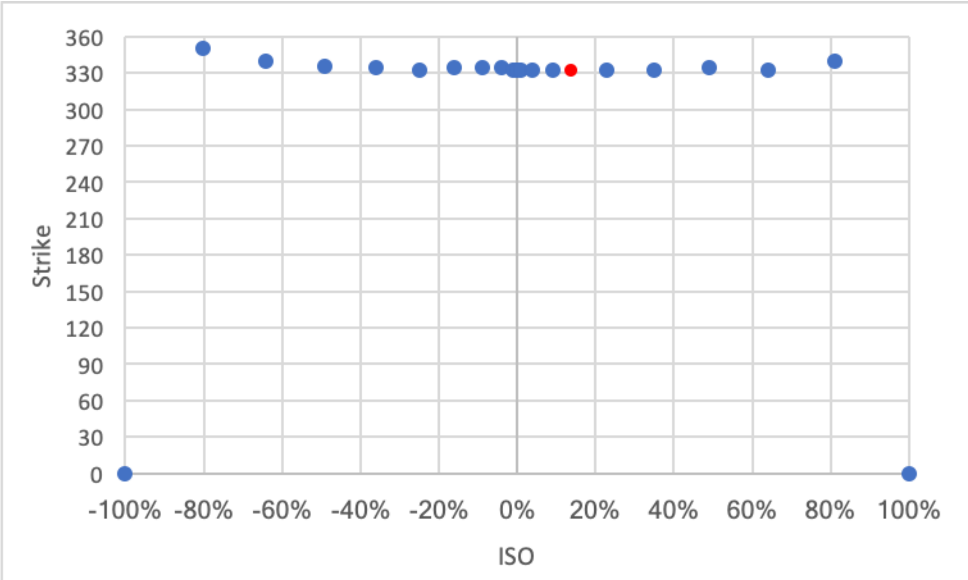

Figure 4.19. Changes in the strike angle with respect to manipulated percentages of ISO are shown as a result of inversions. In this case, stations are placed at 10 and 15 km distances and red dot in the graph shows the original moment tensor with 14% isotropy. The inversions of moment tensor are done for some forced values of ISO%-percentage, which is shown in the x-axis, and the strike angles of the inverted moment tensors are shown in the y-axis.

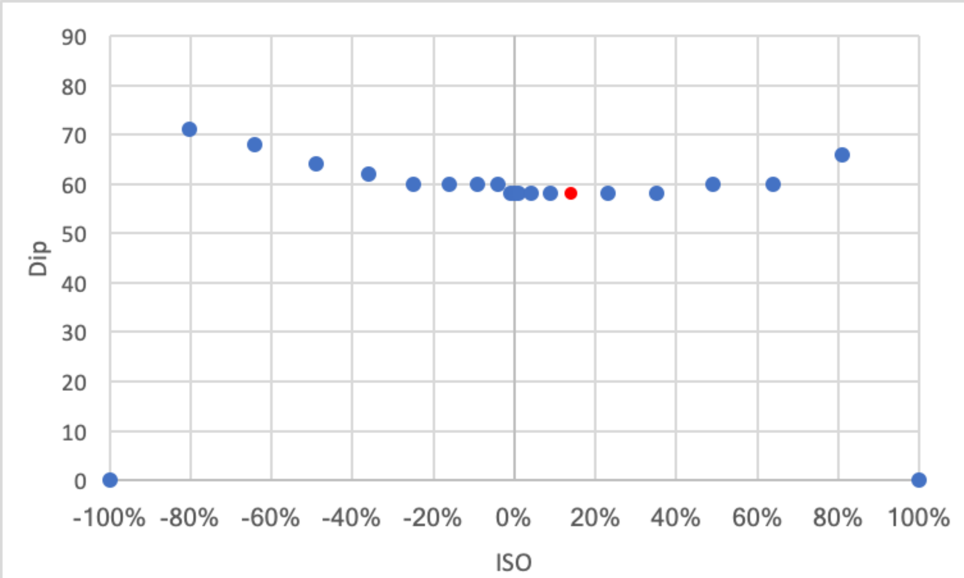

Figure 4.20. Changes in the dip angle with respect to manipulated percentages of ISO are shown as a result of inversions. In this case, stations are placed at 10 and 15 km distances and red dot in the graph shows the original moment tensor with 14% isotropy. The inversions of moment tensor are done for some forced values of ISO%-percentage, which is shown in the x-axis, and the dip angles of the inverted moment tensors are shown in the y-axis.

For figure 4.19, 4.20 and 4.21, the results are expected same. Isotropic percentage should not change the values of strike-dip-rake. In fact, strike-dip-rake are derived from the double couple component of moment tensor, not the isotropic component of moment tensor.

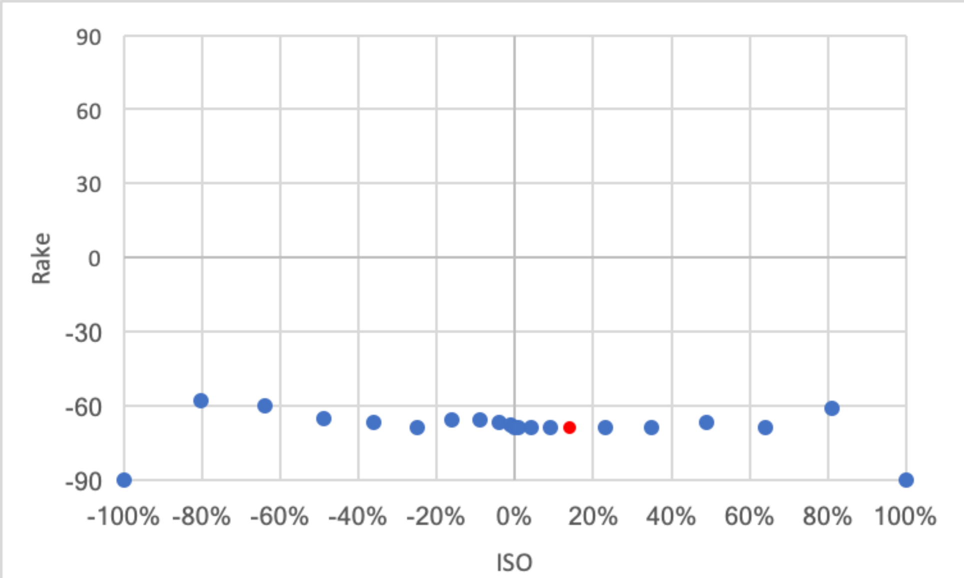

Figure 4.21. Changes in the rake angle with respect to manipulated percentages of ISO are shown as a result of inversions. In this case, stations are placed at 10 and 15 km distances and red dot in the graph shows the original moment tensor with 14% isotropy. The inversions of moment tensor are done for some forced values of ISO%-percentage, which is shown in the x-axis, and the rake angles of the inverted moment tensors are shown in the y-axis.

4.3.2. Stations at 45 km and 80 km for 14% isotropy

In this case, ten stations are placed in a circle with 10 km radius and other ten stations placed in a circle which is 15 km far from the source point. Table 4.6 shows the initial values of the moment tensor and its inverted results. Inversion results are obtained without imposing any parameters such as ζ and χ, which defines the percentages of ISO and CLVD.

Table 4.6. Initial values and inversion results of an earthquake parameters with 99.7 variance reduction in the stations, which are placed at circles with 45 and 85 km radius for the case 3.

Case 3.2	M_0	M_w	Strike	Dip	Rake	ISO%	DC%	CLVD%	ζ	χ
Initial	7.93E+20	3.20	328	56	-74	13.974	85.105	0.921	0.374	-0.103
Inverted	7.041E+20	3.19	328	55	-74	13.970	85.106	0.924	0.370	-0.100

Variance reduction is obtained as 98.4% as a result of inversion. Moment tensor and its parameters are represented in equation 4.12 and Table 4.6.

$$\mathbf{M^{inv}} = \begin{bmatrix} 5.488 & 4.280 & 0.569 \\ 4.280 & 5.528 & 2.495 \\ 0.569 & 2.495 & -3.783 \end{bmatrix} \tag{4.12}$$

Afterwards, inversion parameters are manipulated for the different isotropic percentages (different ζ values). More precisely, apart from the original ζ value of the moment tensor, other possible values of ζ are forced in the range of -1 to 1 with the step of 0.1. Totally 21 inversions are performed for the changing ζ values.

As a result of inversions, results are shown in the Figures 4.22, 4.23, 4.24, 4.25. Figure 4.22 shows how the variance reduction changes as the isotropic percentage varies. These plots show the sensitivity of the inversion to isotropic percentage of the moment tenor. In figures 4.23, 4.24, 4.25, the changes in strike, dip and rake angles are shown according to the variation of isotropic percentages in the range of -100% and 100%.

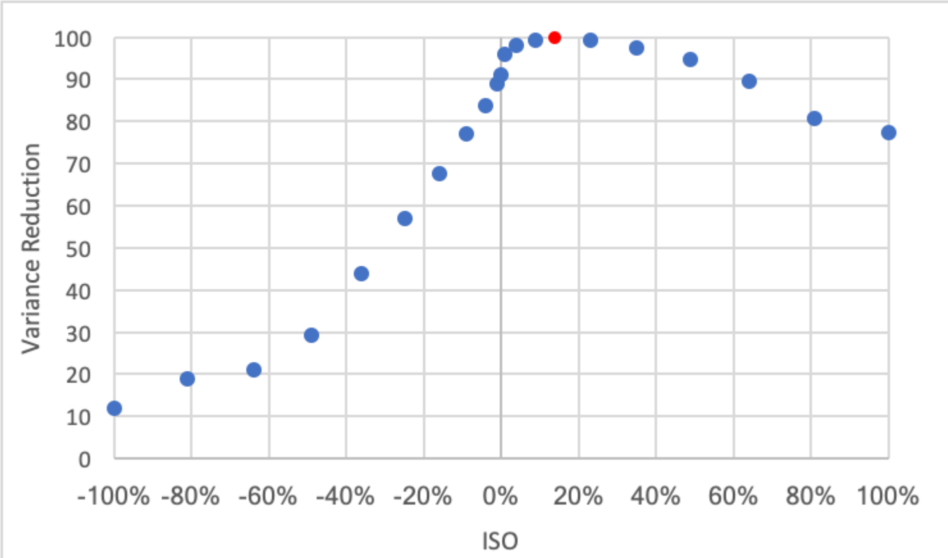

Figure 4.22. As a result of inversions, changes in the variance reduction with respect to manipulated percentages of ISO are shown. In this case, stations are placed at 45 and 80 km distances. The original moment tensor, which is expressed as red dot, has 14% isotropy. The inversions of moment tensor are done for some forced values of ISO%-percentage, which is shown in the x-axis, and the variance reduction values of the inverted moment tensors are shown in the y-axis.

Figure 4.22 reveals the fault that waveforms are not very sensitive to the isotropic component i.e even though the isotropic percentage has approximately 20% error, the synthetic waveforms fit the data by 95% (variance reduction).

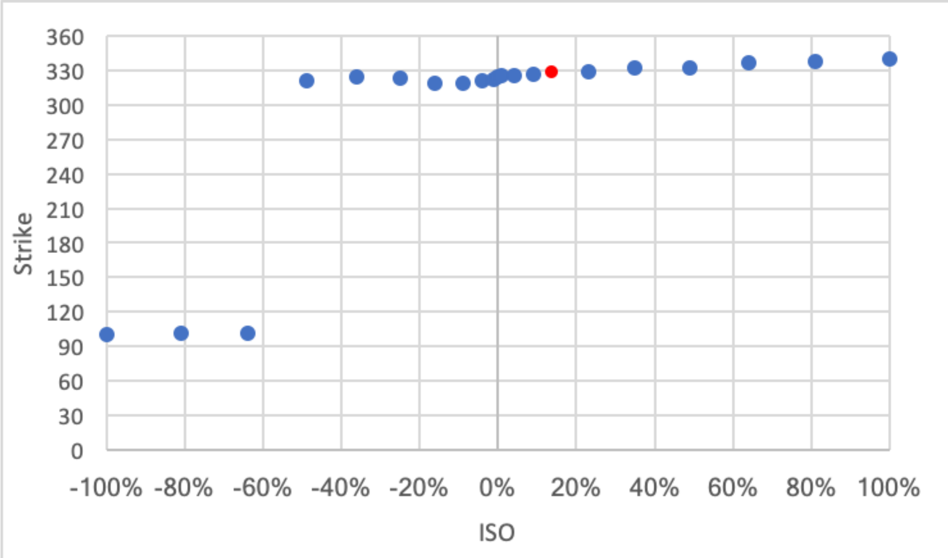

Figure 4.23. Changes in the strike angle with respect to manipulated percentages of ISO are shown as a result of inversions. In this case, stations are placed at 45 and 80 km distances and red dot in the graph shows the original moment tensor with 14% isotropy. The inversions of moment tensor are done for some forced values of ISO%-percentage, which is shown in the x-axis, and the strike angles of the inverted moment tensors are shown in the y-axis.

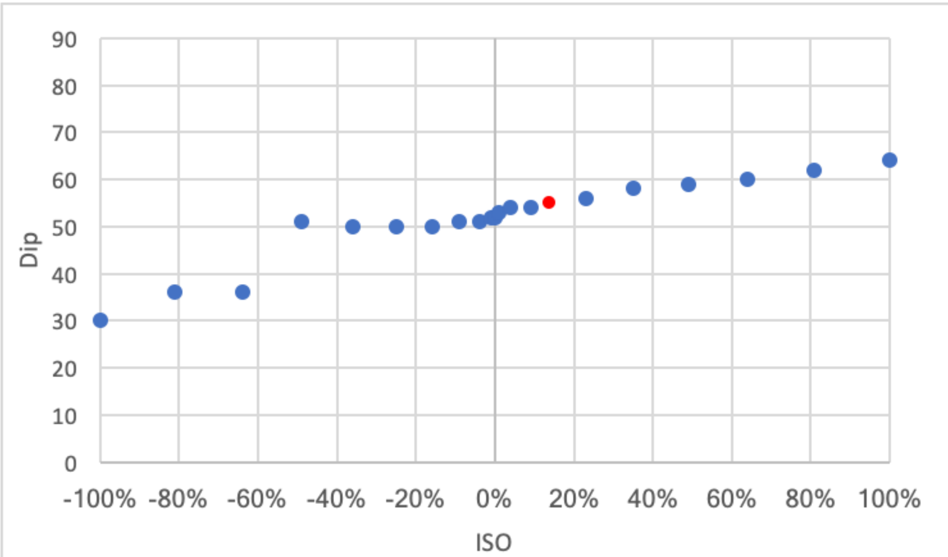

Figure 4.24. Changes in the dip angle with respect to manipulated percentages of ISO are shown as a result of inversions. In this case, stations are placed at 45 and 80 km distances and red dot in the graph shows the original moment tensor with 14% isotropy. The inversions of moment tensor are done for some forced values of ISO%-percentage, which is shown in the x-axis, and the dip angles of the inverted moment tensors are shown in the y-axis.

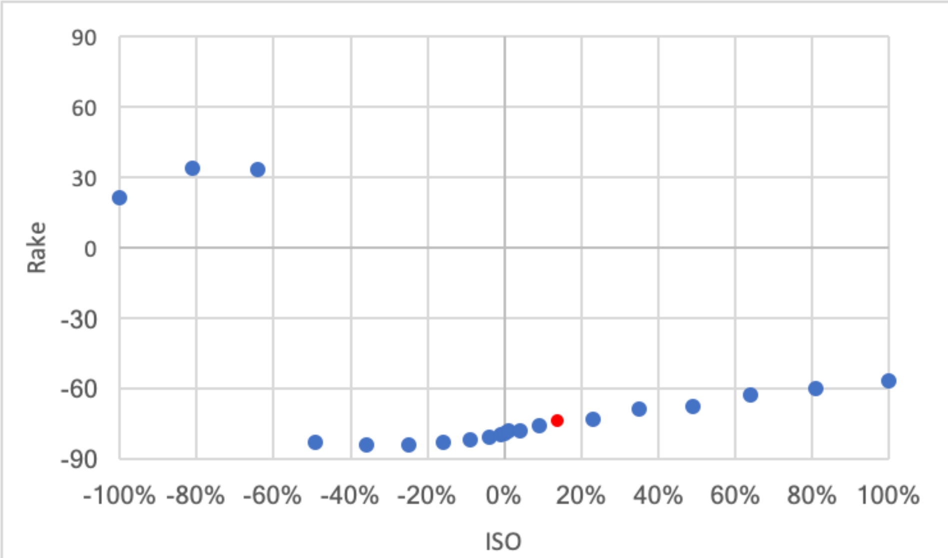

Figure 4.25. Changes in the rake angle with respect to manipulated percentages of ISO are shown as a result of inversions. In this case, stations are placed at 45 and 80 km distances and red dot in the graph shows the original moment tensor with 14% isotropy. The inversions of moment tensor are done for some forced values of ISO%-percentage, which is shown in the x-axis, and the rake angles of the inverted moment tensors are shown in the y-axis.

For figure 4.23, 4.24 and 4.25, the results are expected same. Isotropic percentage should not change the values of strike-dip-rake. In fact, strike-dip-rake are derived from the double couple component of moment tensor, not the isotropic component of moment tensor.

4.4. Changing the hypocentral depth

In this section inversion processes are manipulated for different hypocentral depths of 3 different earthquakes with 2%, 5% and 14% isotropy and 2 sets od circles of stations, which are located at 45 and 80 km distances and each circle has ten stations are used for each inversion.

Originally, hypocentral depths of the 3 different types earthquakes are set as 8 km. Afterwards, inversions are performed in every 0.5 meters from 0.5 meters depth to 20 meters for each case. As a result of those manipulated inversions of earthquakes at different depths, the changes in isotropic percentages and the corresponding variance reduction values are ploted in Figures 4.26, 4.28, 4.30.

4.4.1. Changing the hypocentral depth for the inversion with 2% isotropy

In this case, total 20 stations are placed in the two circles at 45 and 80 km far from the source point to the inversion. Firstly, generated moment tensor (equation 4.1), which has 2% isotropy, is inverted at its original hypocentral depth (8 km). After that, inversion process is manipulated for different depth values from 0.5 km to 20 km with a stepsize of 0.5 km for the same earthquake. In other words, only the hypocentral depth of the original earthquake is changed in order to observe changes in isotropic perentages and variance reduction values.

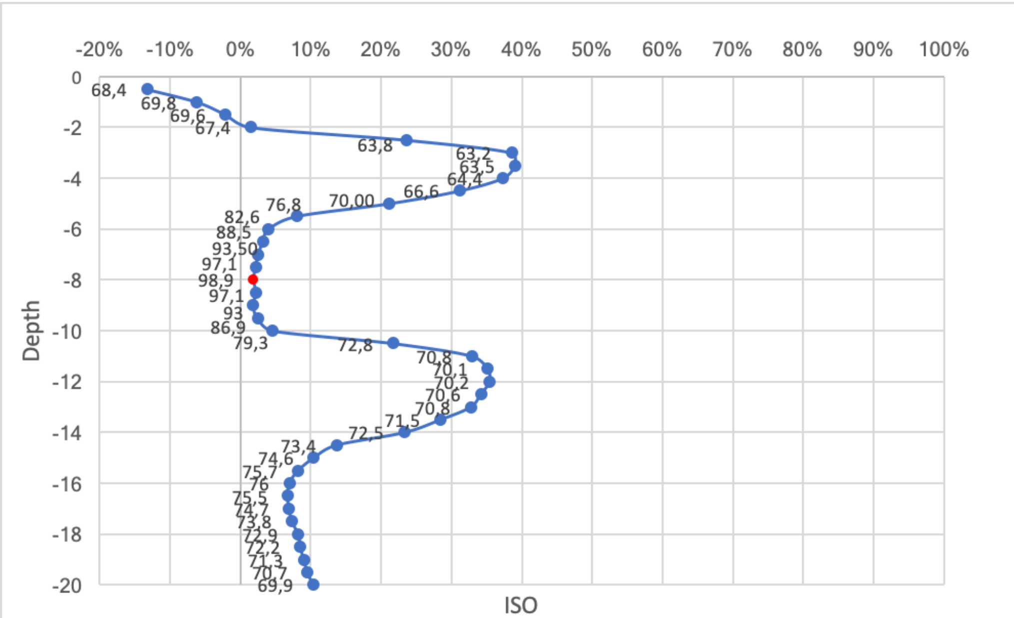

Figure 4.26. Changes in the isotropic percentages are shown with respect to manipulated hypocentral depth as a result of inversions. In this case, the original moment tensor has 2% isotropy and stations are located at 45 and 80 km distances. Red dot shows the original result from the inversion and the values. The variance reduction for each inversion is shown at the left-hand side of the dots.

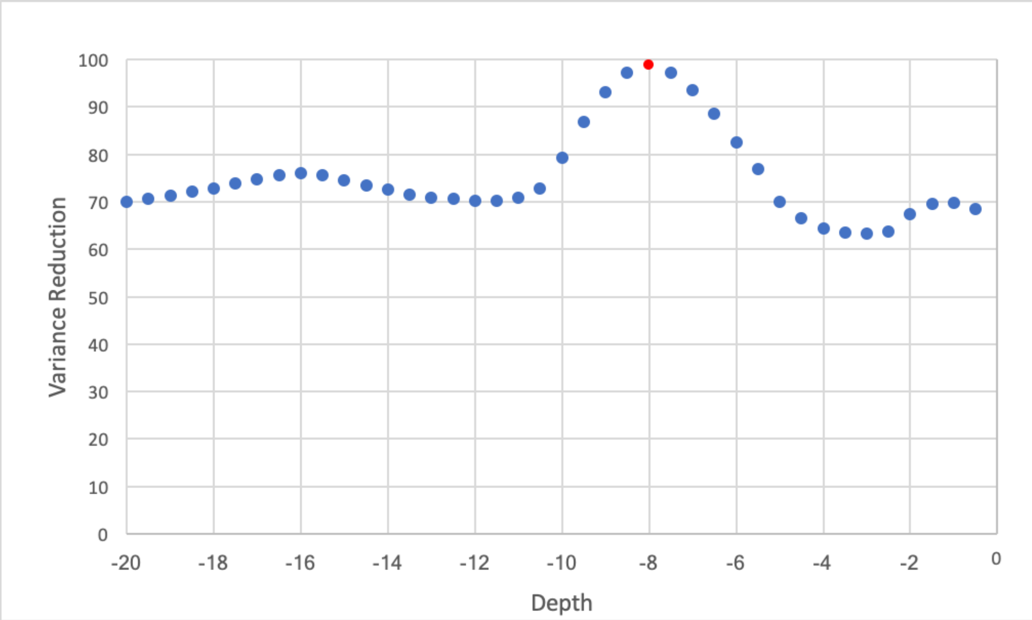

Figure 4.27. As a result of inversions, changes in the variance reduction depends on changing hypocentral depth are shown. Red dot represents the original inversions result of moment tensor with 2% isotropy.

As a result of inversions, findings are shown in the Figures 4.26 and 4.27. In Figure 4.26, changes in the isotropic percentages with respect to manipulated hypocentral depth and variance reduction values for each case are shown. Moreover, changes in the variance reduction depends on changing hypocentral depth are expressed in Figure 4.27 as a result of total 40 inversions.

4.4.2. Changing the hypocentral depth for the inversion with 5% isotropy

In this case, total 20 stations are placed in the two circles at 45 and 80 km far from the source point to the inversion. Firstly, generated moment tensor (equation 4.5), which has 5% isotropy, is inverted at its original hypocentral depth (8 km). After that, inversion process is manipulated for different depth values from 0.5 km to 20 km with a stepsize of 0.5 km for the same earthquake mechanism. In other words, only the hypocentral depth of the original earthquake is changed in order to observe changes in isotropic perentages and variance reduction values.

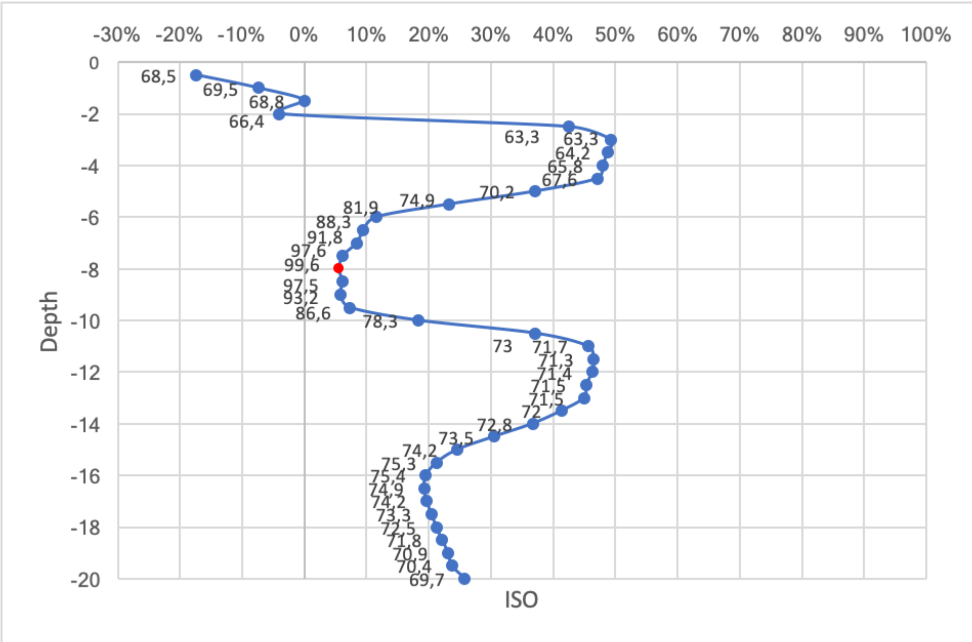

Figure 4.28. Changes in the isotropic percentages are shown with respect to manipulated hypocentral depth as a result of inversions. In this case, the original moment tensor has 5% isotropy and stations are located at 45 and 80 km distances. Red dot shows the original result from the inversion and the values. The variance reduction for each inversion is shown at the left-hand side of the dots.

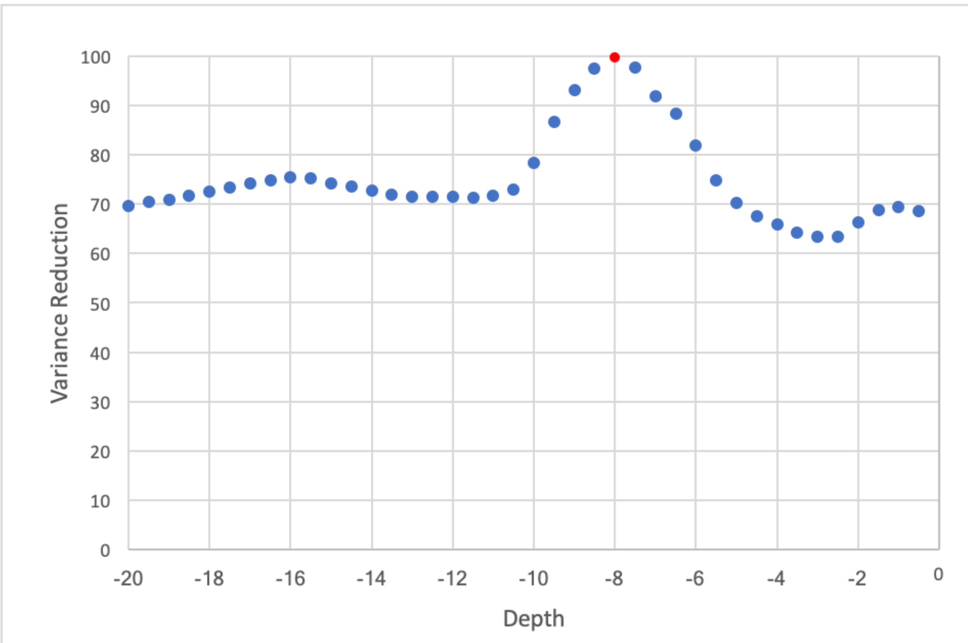

Figure 4.29. As a result of inversions, changes in the variance reduction depends on changing hypocentral depth are shown. Red dot represents the original inversions result of moment tensor with 5% isotropy.

As a result of inversions, findings are shown in the Figures 4.28 and 4.29. In Figure 4.28, changes in the isotropic percentages with respect to manipulated hypocentral depth and variance reduction values for each case are shown. Moreover, changes in the variance reduction depends on changing hypocentral depth are expressed in Figure 4.29 as a result of total 40 inversions.

4.4.3. Changing the hypocentral depth for the inversion with 14% isotropy

In this case, total 20 stations are placed in the two circles at 45 and 80 km far from the source point to the inversion. Firstly, generated moment tensor (equation 4.9), which has 14% isotropy, is inverted at its original hypocentral depth (8 km). After that, inversion process is manipulated for different depth values from 0.5 km to 20 km with a stepsize of 0.5 km for the same earthquake mechanism. In other words, only the hypocentral depth of the original earthquake is changed in order to observe changes in isotropic perentages and variance reduction values.

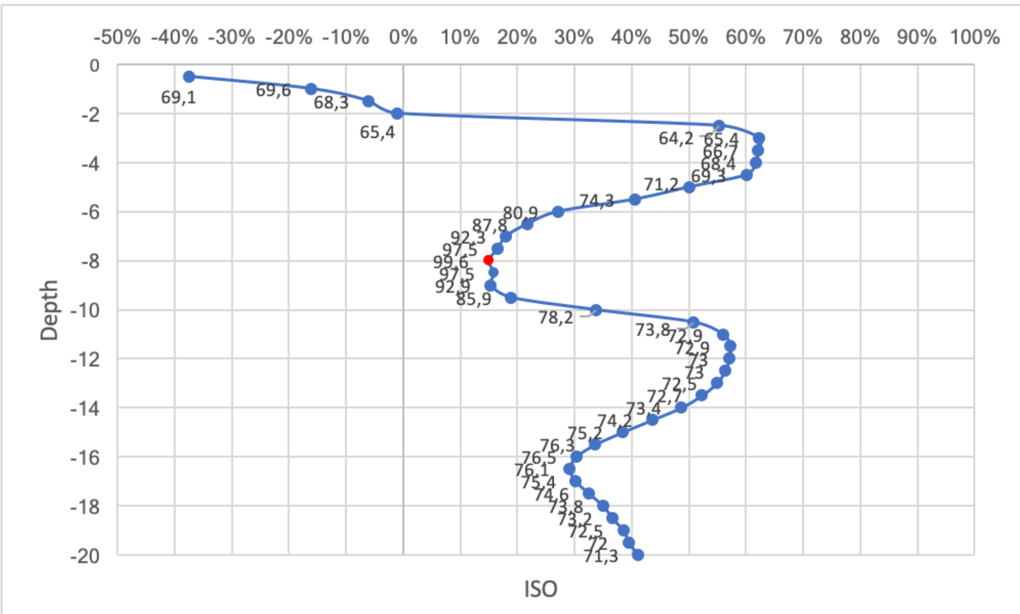

Figure 4.30. Changes in the isotropic percentages are shown with respect to manipulated hypocentral depth as a result of inversions. In this case, the original moment tensor has 14% isotropy and stations are located at 45 and 80 km distances. Red dot shows the original result from the inversion and the values. The variance reduction for each inversion is shown at the left-hand side of the dots.

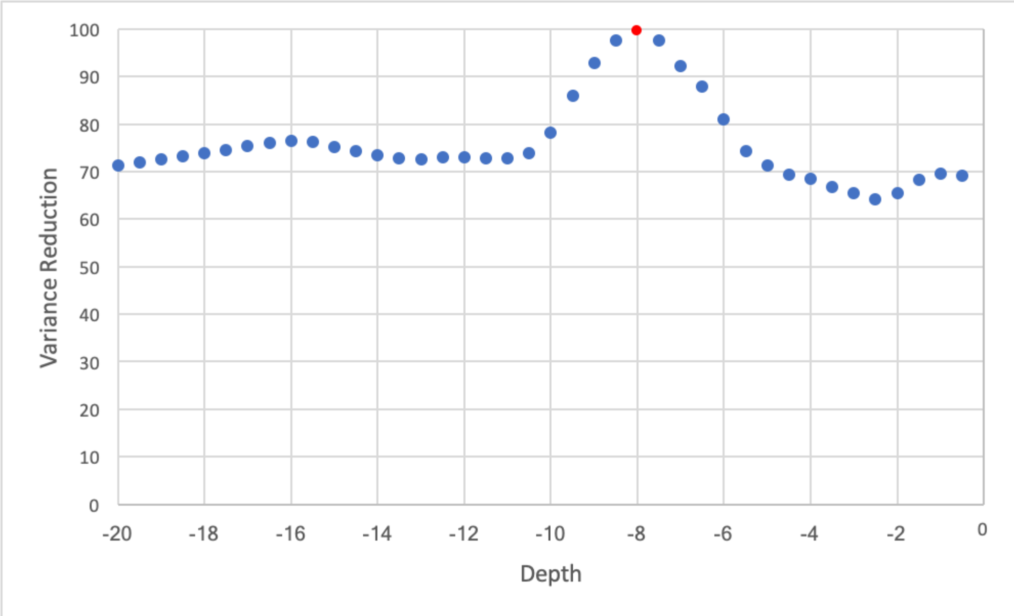

Figure 4.31. As a result of inversions, changes in the variance reduction depends on changing hypocentral depth are shown. Red dot represents the original inversions result of moment tensor with 14% isotropy.

As a result of inversions, findings are shown in the Figures 4.30 and 4.31. In Figure 4.30, changes in the isotropic percentages with respect to manipulated hypocentral depth and variance reduction values for each case are shown. Moreover, changes in the variance reduction depends on changing hypocentral depth are expressed in Figure 4.31 as a result of total 40 inversions.

5. DISCUSSION AND CONCLUSIONS

In this chapter, results are considered and compared to each other in terms of changing isotropic percentages, depth, variance reduction and waveforms in distributed stations. Locations of the stations are mentioned in Figure 4.1, and synthetic waveforms are shown in 10 different azimuthal locations for each case. Mainly, 3 different earthquakes with 2%, 5% and 14% isotropy and correspondingly 3 different stations set (at 15, 45, 80 km distances) are used. Moreover, inversion results of those synthetic earthquakes are examined in terms of depth, isotropic percentage and variance reduction value.

5.1. Case 1: Waveforms of the synthetic earthquake with 2% isotropy

In this case, mainly generated synthetic moment tensor and its isotropic and deviatoric part are shown separately. There are totally 10 stations, which are located at 15, 45 and 80 km far away from the source and the Figures 5.1, 5.2, 5.3 show the distribution of the stations. For this case, moment tensor with 2% isotropy in equation 4.1 is shown as waveform and also it is divided into its components namely isotropic and deviatoric. In each stations, waveforms are scaled by amplitude of isotropic parts of the moment tensor and all of these data are shown without any filters.

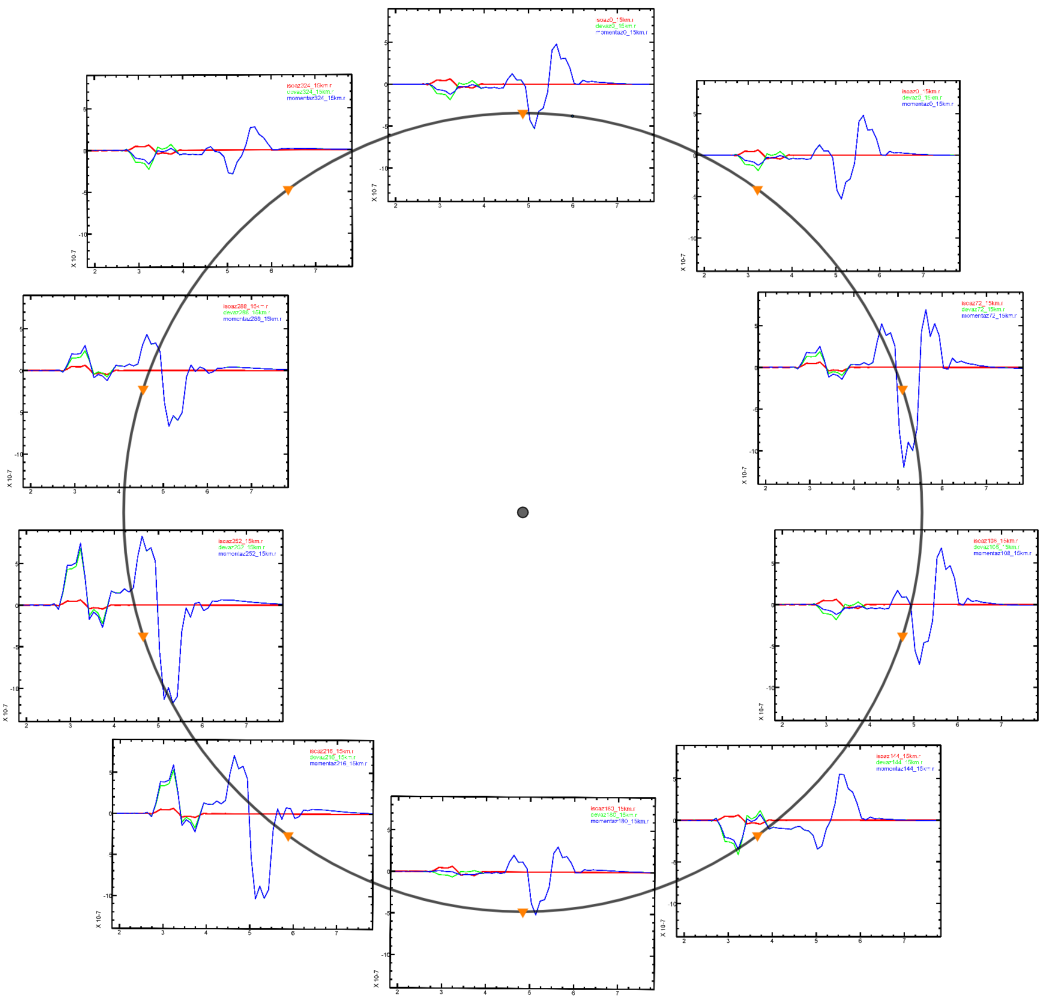

Figure 5.1. Waveforms of the unfiltered earthquakes data are shown. In this case, stations are located at 15 km and moment tensor has 2% isotropy component. Additionally, waveforms are differentiated with colors; red lines, green lines and blue lines express the isotropic part, deviatoric part and moment tensor itself respectivelty.

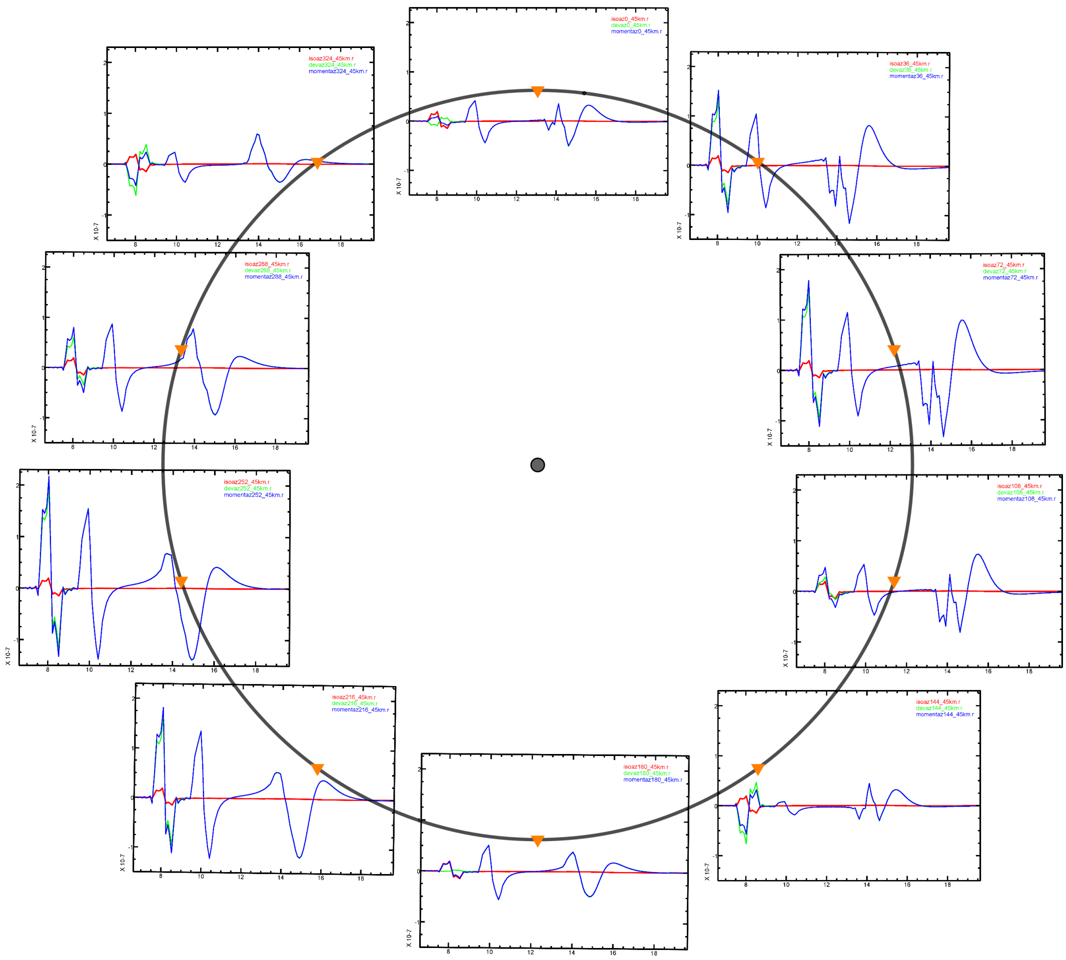

Figure 5.2. Waveforms of the unfiltered earthquakes data are shown. In this case, stations are located at 45 km and moment tensor has 2% isotropy component. In this figure, waveforms are differentiated with colors; red lines, green lines and blue lines express the isotropic part, deviatoric part and moment tensor itself respectivelty.

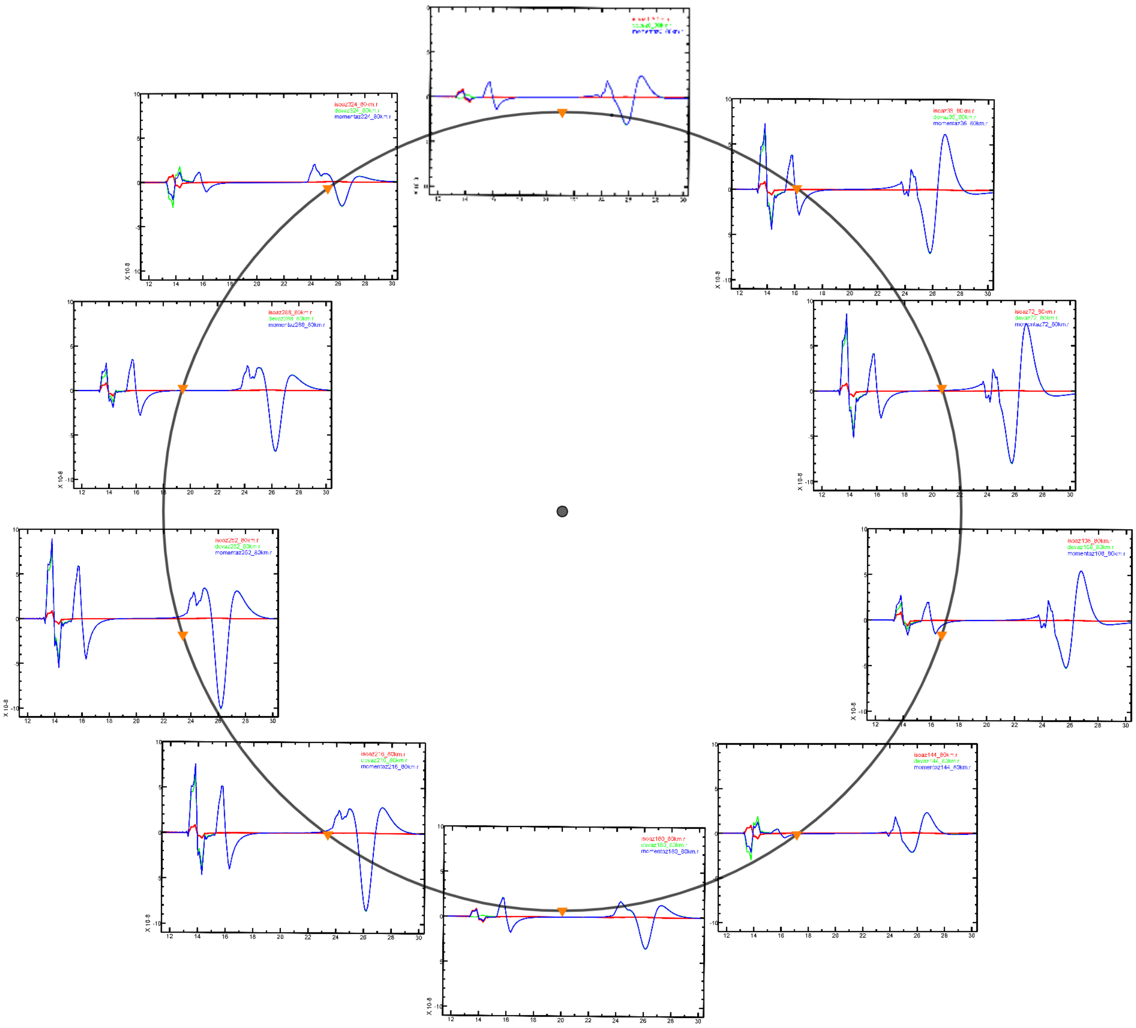

Figure 5.3. Waveforms of the unfiltered earthquakes data are shown. In this case, stations are located at 80 km and moment tensor has 2% isotropy component. In this figure, waveforms are differentiated with colors; red lines, green lines and blue lines express the isotropic part, deviatoric part and moment tensor itself respectivelty.

5.2. Case 2: Waveforms of the synthetic earthquake with 5% isotropy

In this case, mainly generated synthetic moment tensor and its isotropic and deviatoric part are shown separately. There are totally 10 stations, which are located at 15, 45 and 80 km far away from the source and the Figures 5.4, 5.5, 5.6 show the distribution of the stations. For this case, moment tensor with 5% isotropy in equation 4.5 is shown as waveform and also it is divided into its components namely isotropic and deviatoric. In each stations, waveforms are scaled by amplitude of isotropic parts of the moment tensor and all of these data are shown without any filters.

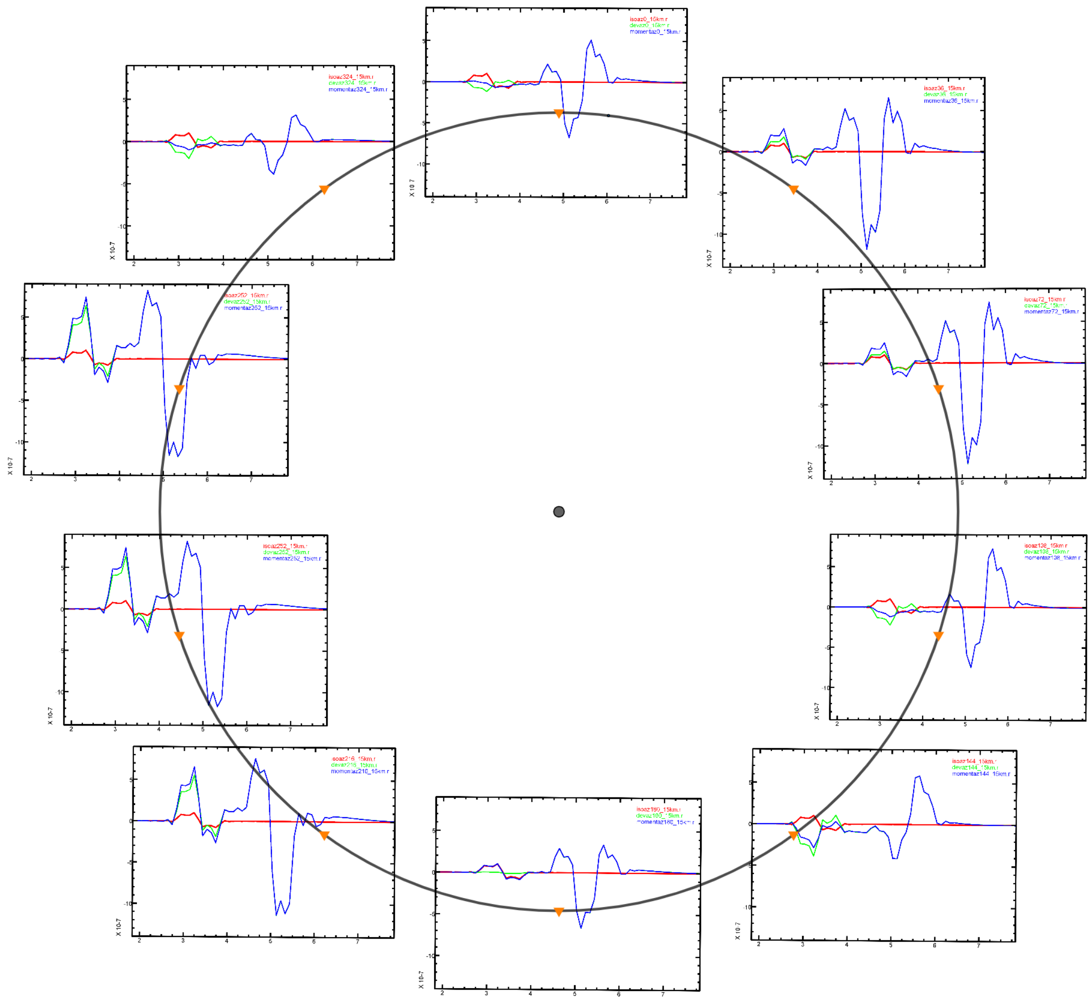

Figure 5.4. Waveforms of the unfiltered earthquakes data are shown. In this case, stations are located at 15 km and moment tensor has 5% isotropy component. In this figure, waveforms are differentiated with colors; red lines, green lines and blue lines express the isotropic part, deviatoric part and moment tensor itself respectivelty.

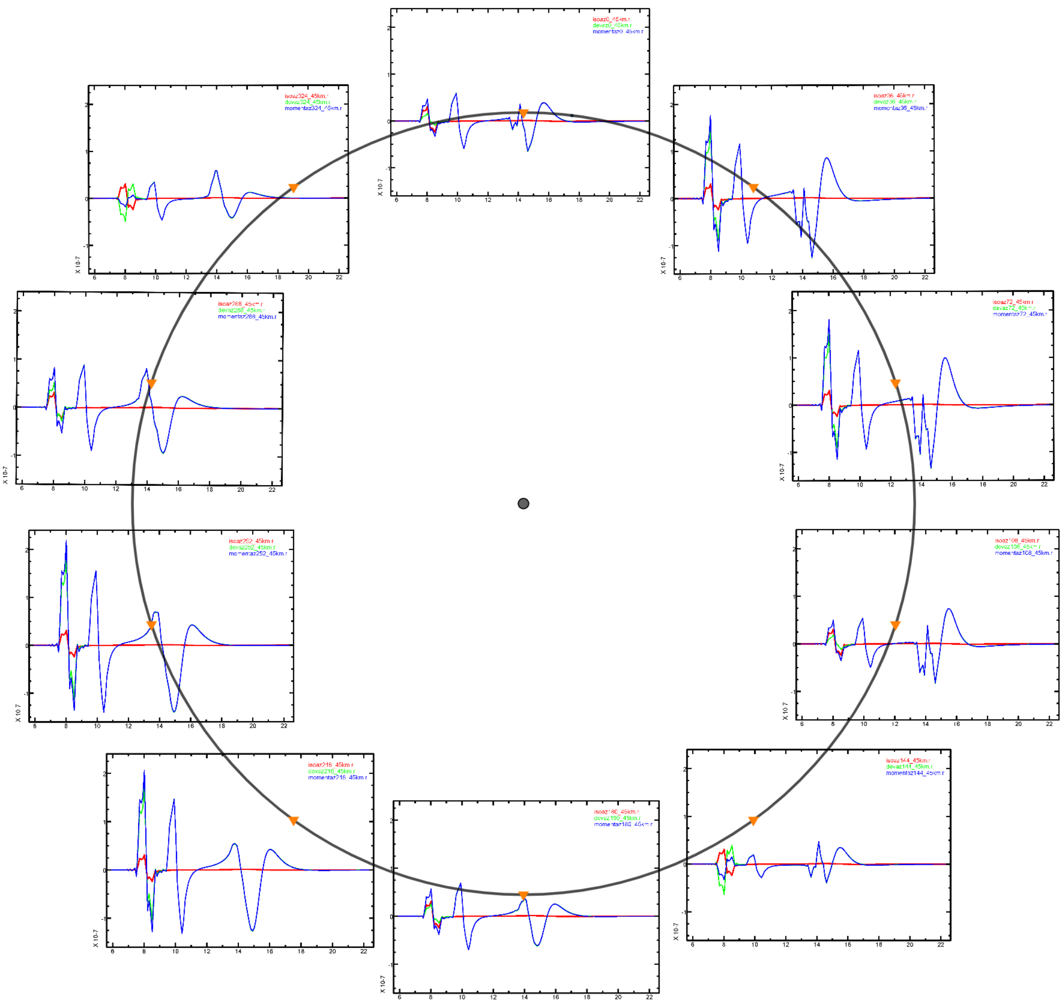

Figure 5.5. Waveforms of the unfiltered earthquakes data are shown. In this case, stations are located at 45 km and moment tensor has 5% isotropy component. In this figure, waveforms are differentiated with colors; red lines, green lines and blue lines express the isotropic part, deviatoric part and moment tensor itself respectivelty.

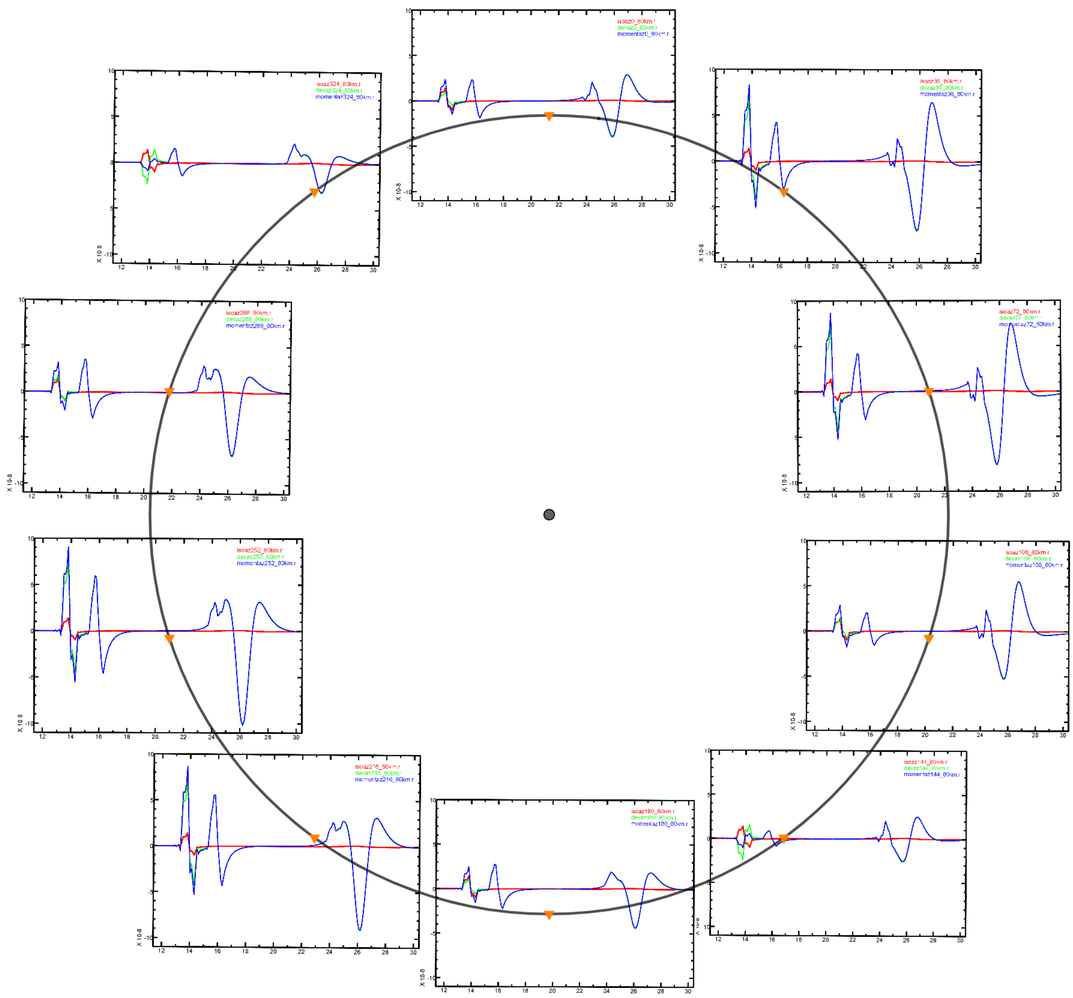

Figure 5.6. Waveforms of the unfiltered earthquakes data are shown. In this case, stations are located at 80 km and moment tensor has 5% isotropy component. In this figure, waveforms are differentiated with colors; red lines, green lines and blue lines express the isotropic part, deviatoric part and moment tensor itself respectivelty.

5.3. Case 3: Waveforms of the synthetic earthquake with 14% isotropy

In this case, mainly generated synthetic moment tensor and its isotropic and deviatoric part are shown separately. There are totally 10 stations, which are located at 15, 45 and 80 km far away from the source and the Figures 5.7, 5.8, 5.9 show the distribution of the stations. For this case, moment tensor with 14% isotropy in equation 4.9 is shown as waveform and also it is divided into its components namely isotropic and deviatoric. In each stations, waveforms are scaled by amplitude of isotropic parts of the moment tensor and all of these data are shown without any filters.

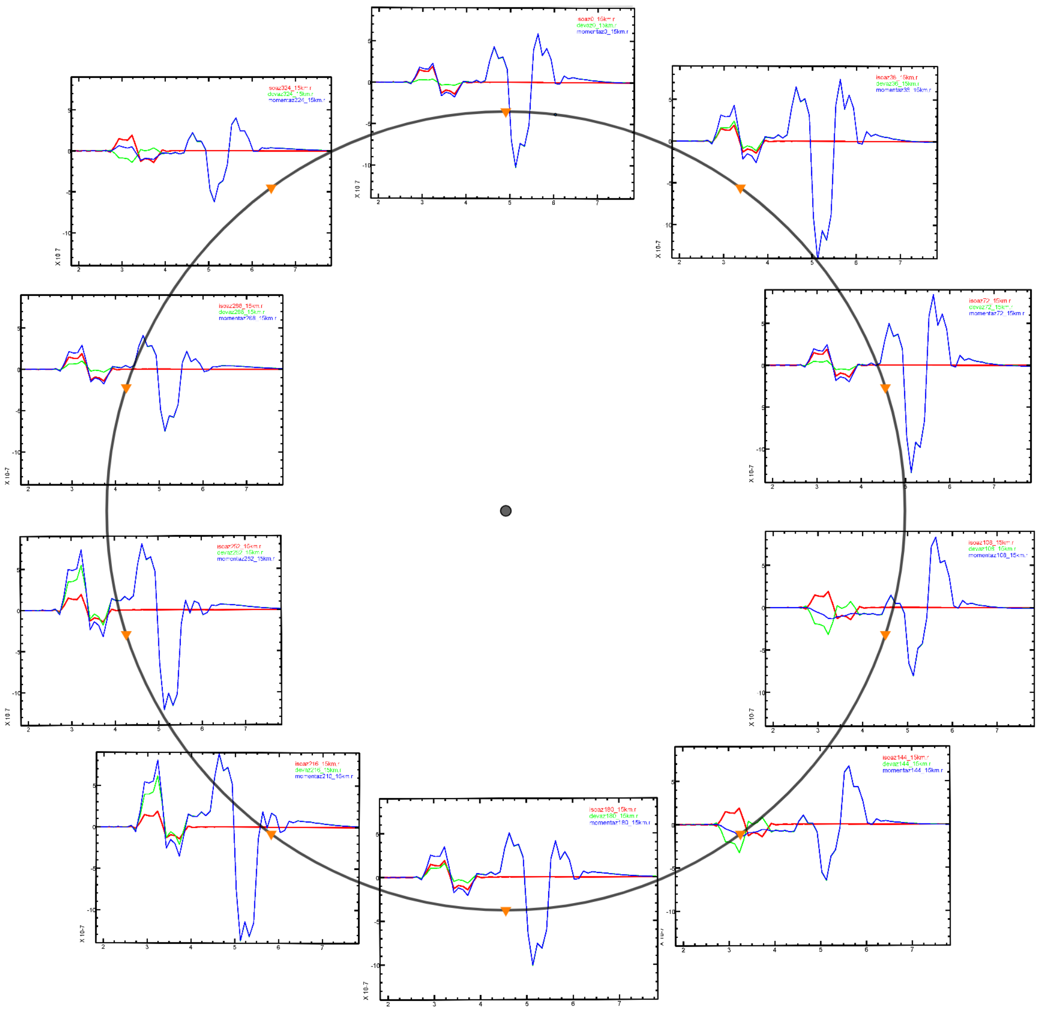

Figure 5.7. Waveforms of the unfiltered earthquakes data are shown. In this case, stations are located at 15 km and moment tensor has 14% isotropy component. In this figure, waveforms are differentiated with colors; red lines, green lines and blue lines express the isotropic part, deviatoric part and moment tensor itself respectivelty.

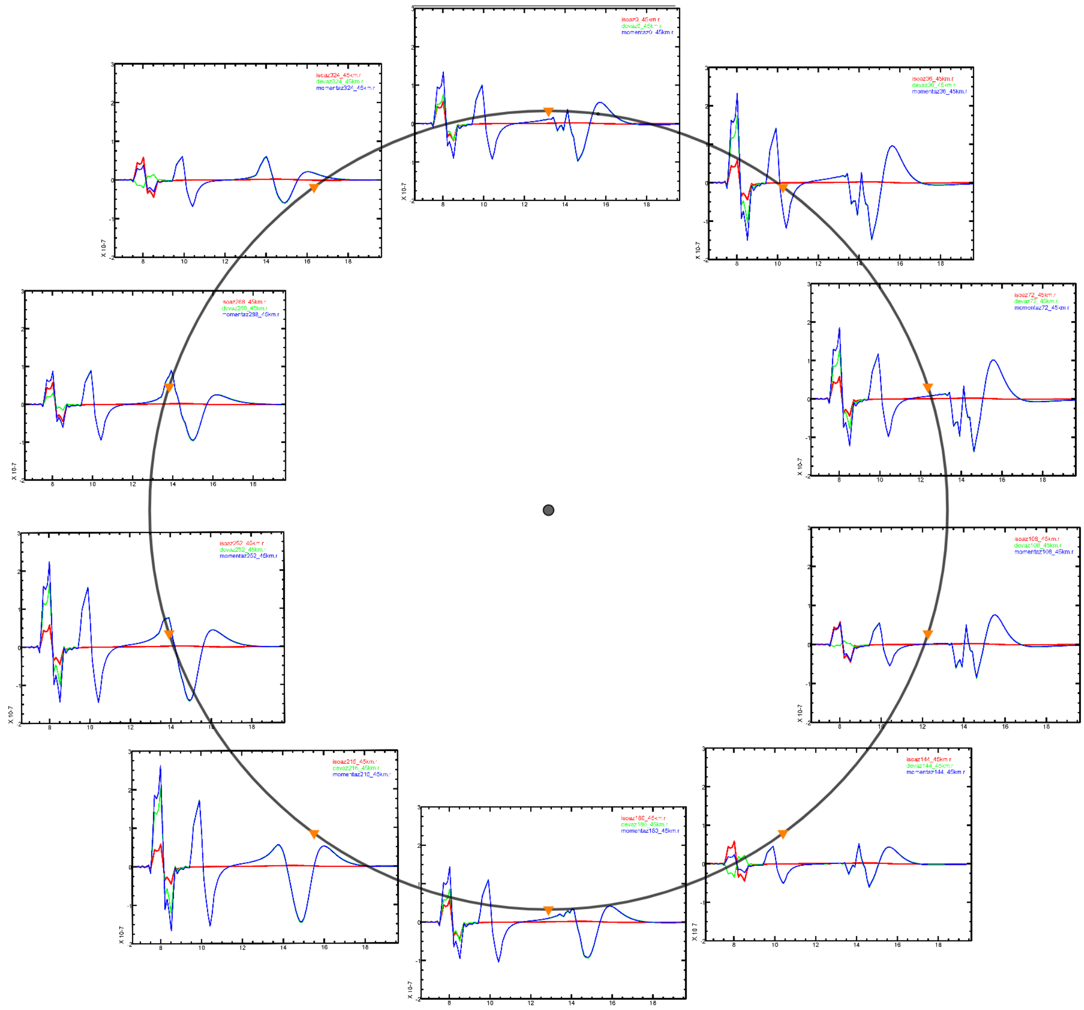

Figure 5.8. Waveforms of the unfiltered earthquakes data are shown. In this case, stations are located at 45 km and moment tensor has 14% isotropy component. In this figure, waveforms are differentiated with colors; red lines, green lines and blue lines express the isotropic part, deviatoric part and moment tensor itself respectivelty.

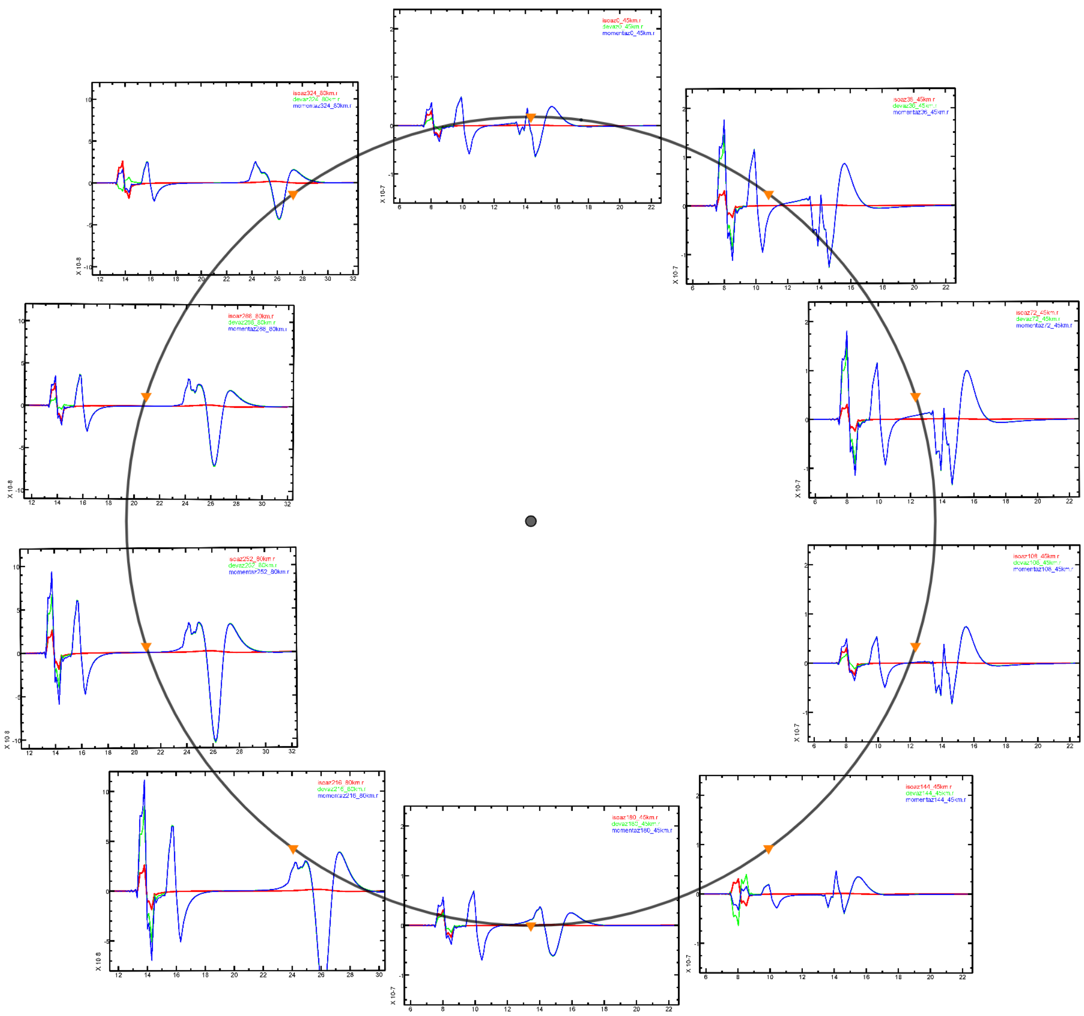

Figure 5.9. Waveforms of the unfiltered earthquakes data are shown. In this case, stations are located at 80 km and moment tensor has 14% isotropy component. In this figure, waveforms are differentiated with colors; red lines, green lines and blue lines express the isotropic part, deviatoric part and moment tensor itself respectivelty.

At this point, different isotropic percentages (2%, 5% and 14%) in the waveforms are shown at stations which are located at different distances (15, 45 and 80 km) and azimuths. In the light of those findings, one can notice that isotropy component has small energy compared to the whole waveform. Inversion of the isotropic component is very small part when it is compared to the inversion of the full waveform because there are only small amount of isotropy part involves in P-wave.

As a result of those Figures mentioned above, inversion is not really sensitive to isotropic percentage in the moment tensor. Even though the error of isotropic value increases, variance reduction can be very high because the ratio of isotropy in the full waveform is very low.

5.4. How does variance reduction change with respect to different isotropic percentages ?

Firstly, inversion results of the moment tensor with 2% isotropy are recorded at two different sets of stations. Those results are compared to each others. Figure 5.10 shows the effect of manipulated iso percentages (in the inversion processes) on the variance reduction values.

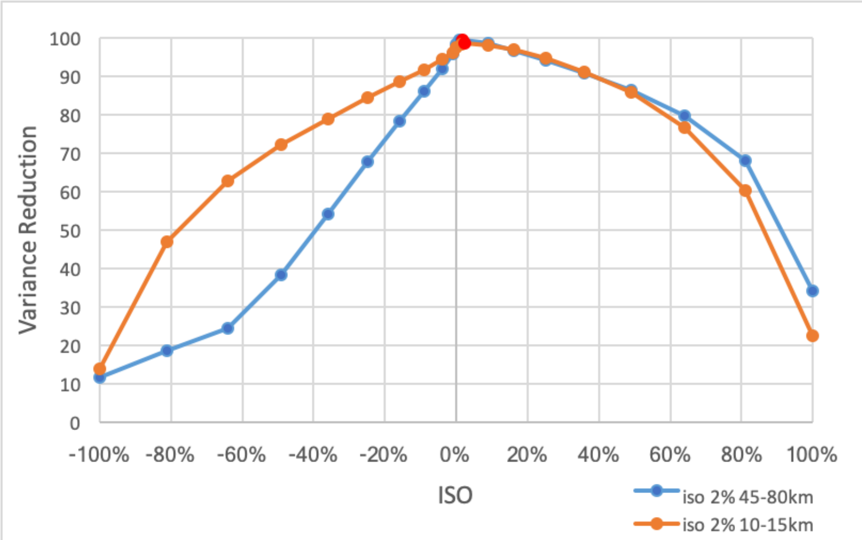

Figure 5.10. As a result of inversions, changes in the variance reduction with respect to manipulated percentages of ISO are shown. In this case, 2 different sets of stations are used seperately. Blue dots indicate the inversion of the moment tensor with 2% isotropy recorded at 45 and 80 km. Orange dots indicate the inversion of the same moment tensor, which is recorded at 10 and 15 km.

Secondly, inversion results of the moment tensor with 5% isotropy are recorded at two different sets of stations. Those results are compared to each others. Figure 5.11 shows the effect of manipulated iso percentages (in the inversion processes) on the variance reduction values.

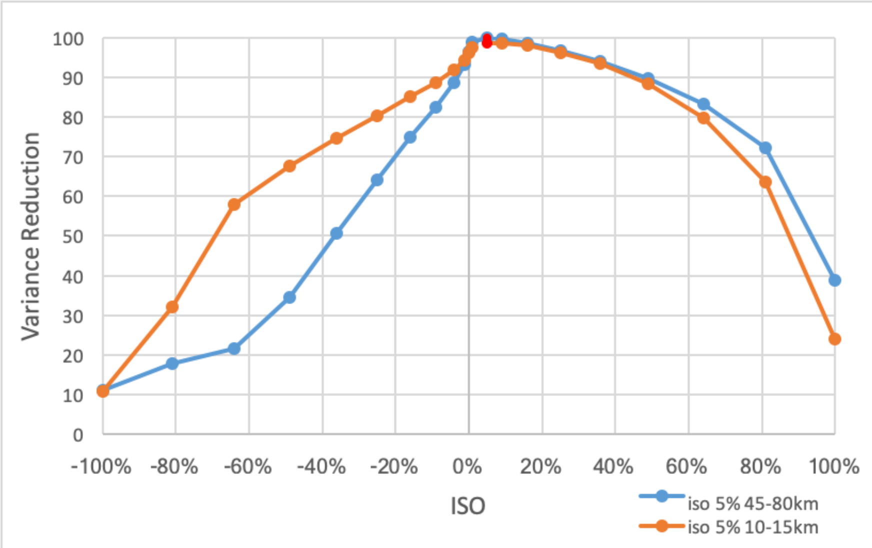

Figure 5.11. As a result of inversions, changes in the variance reduction with respect to manipulated percentages of ISO are shown. In this case, the sets of two different stations are used seperately. Blue dots indicate the inversion of the moment tensor with 5% isotropy recorded at 45 and 80 km. Orange dots indicate the inversion of the same moment tensor, which is recorded at 10 and 15 km.

Thirdly, inversion results of the moment tensor with 14% isotropy are recorded at two different stations sets. Those results are compared to each others. Figure 5.12 shows the effect of manipulated iso percentages (in the inversion processes) on the variance reduction values.

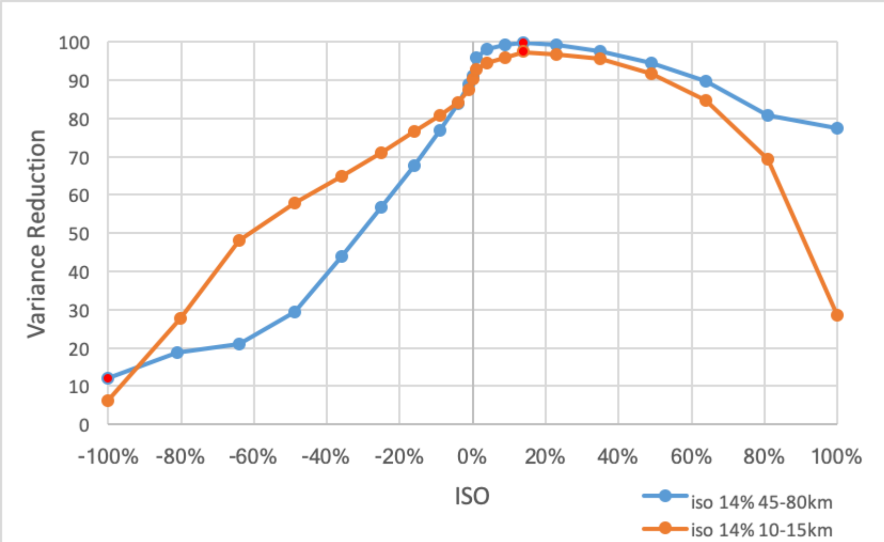

Figure 5.12. As a result of inversions, changes in the variance reduction with respect to manipulated percentages of ISO are shown. In this case, 2 different stations set are used seperately. Blue dots indicate the inversion of the moment tensor with 14% isotropy recorded at 45 and 80 km. Orange dots indicate the inversion of the same moment tensor, which are recorded at 10 and 15 km.

Those three graphics mentioned below (Figures 5.10, 5.11 and 5.12) show that for all cases inversion results are not sensitive when the manipulated isotropic percentages are smaller than 0. Moreover, when the isotropy values are close to the original isotropic percentages (approximately +-5), it can be seen that inversions of the full waveforms recorded at 45 and 80 km give relatively better variance reduction values. Additionally, as the initial values of the isotropic percentages are getting greater (from %2 to 14%), relatively close stations give lower variance reduction values as a result of inversions.

Moreover, inversions of those different moment tensors are also examined together. In Figures 5.13 and 5.14 show the all inversions results of three moment tensors recorded at two different sets of stations. Firstly, inversion results of the moment tensors with 2%, 5% and 14% isotropy are recorded at 10 and 15 km far away from the source location (Figure 5.13). Secondly, same conditions of inversion method is applied to same earthquakes, but different stations, which are located at 45 and 80 km (Figure 5.14). Those results are compared to each others in order to notice the effect of manipulated iso percentages (in the inversion processes) on the variance reduction values.

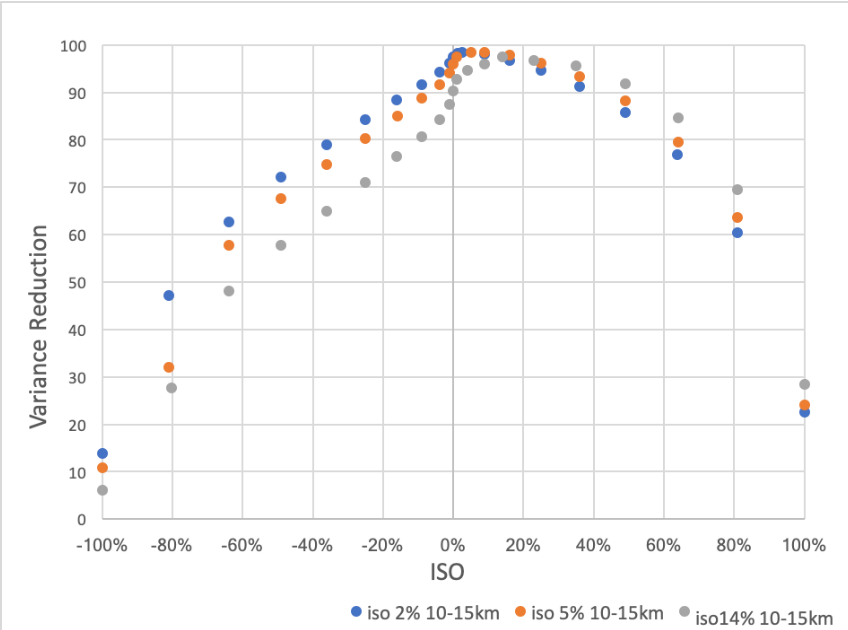

Figure 5.13. As a result of inversions, changes in the variance reduction with respect to manipulated percentages of ISO are shown together for three earthquakes recorded at 10 and 15 km far away from the source locations. Blue dots, orange dots and gray dots indicate the moment tensors with 2%, 5% and 14% isotropy respectively.

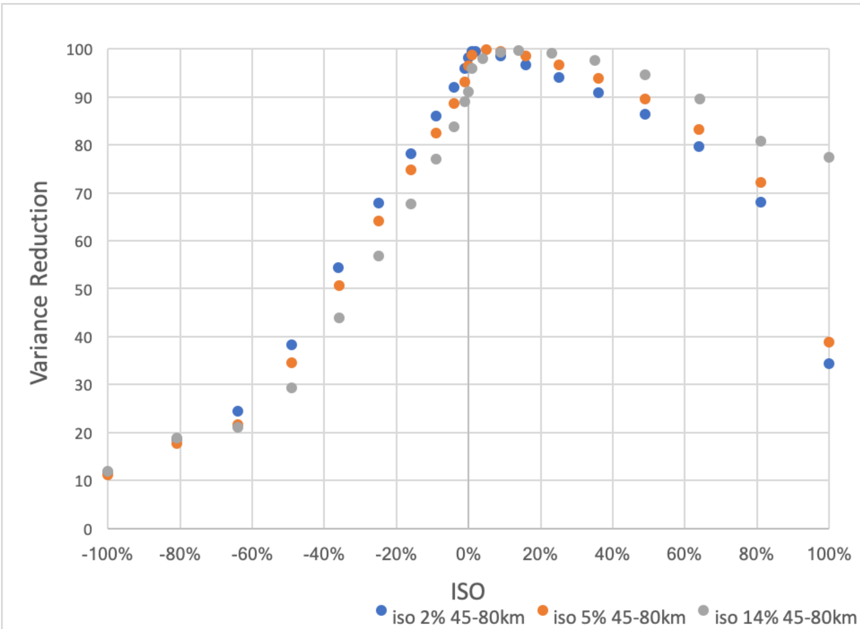

Figure 5.14. As a result of inversions, changes in the variance reduction with respect to manipulated percentages of ISO are shown together for three earthquakes recorded at 45 and 80 km far away from the source locations. Blue dots, orange dots and gray dots indicate the moment tensors with 2%, 5% and 14% isotropy respectively.

In the light of Figures 5.14 and 5.13, earthquakes with a relatively high isotropic percentage give higher variance reduction values when the inversions are performed with larger isotropic percentage than the initial one. In the earthquakes measured at a greater distances (using stations set at 45-80 km), difference becomes even more pronounced in the manner of variance reduction values as a result of inversions.

In the Figure 5.13, when the moment tensor with 14% isotropy is inverted with values greater than the initial value of isotropy, it gives higher variance reduction results than the inversion results of moment tensors with 5% and 2% isotropy. This means that earthquakes with relatively high isotropic percentages are less sensitive when inversions are performed with modified greater isotropic percentages than the initial one.

5.5. How does the error in depth effect the isotropic percentage in the inversion ?

In this section total 20 stations are placed in the two circles at 45 and 80 km far from the source point to the inversion. Firstly, generated moment tensors (equations 4.1, 4.5 and 4.9), which have 2%, 5% and 14% isotropy respectively, are inverted at its original hypocentral depth (8 km) and all the results for changing hypocentral depth are. Originally, hypocentral depths of the 3 different synthetic earthquakes are set as 8 km. However, inversions are performed for different depth values from 0.5 km to 20 km with the step of 0.5 km for each earthquake. In other words, only the hypocentral depths of the original earthquakes are changed in order to observe changes in isotropy perentage and variance reduction values. As a result of those manipulated inversions of synthetic earthquakes at different depths, changes of isotropic percentages and dependently changes in the variance reduction values are considered (Figure 5.15).

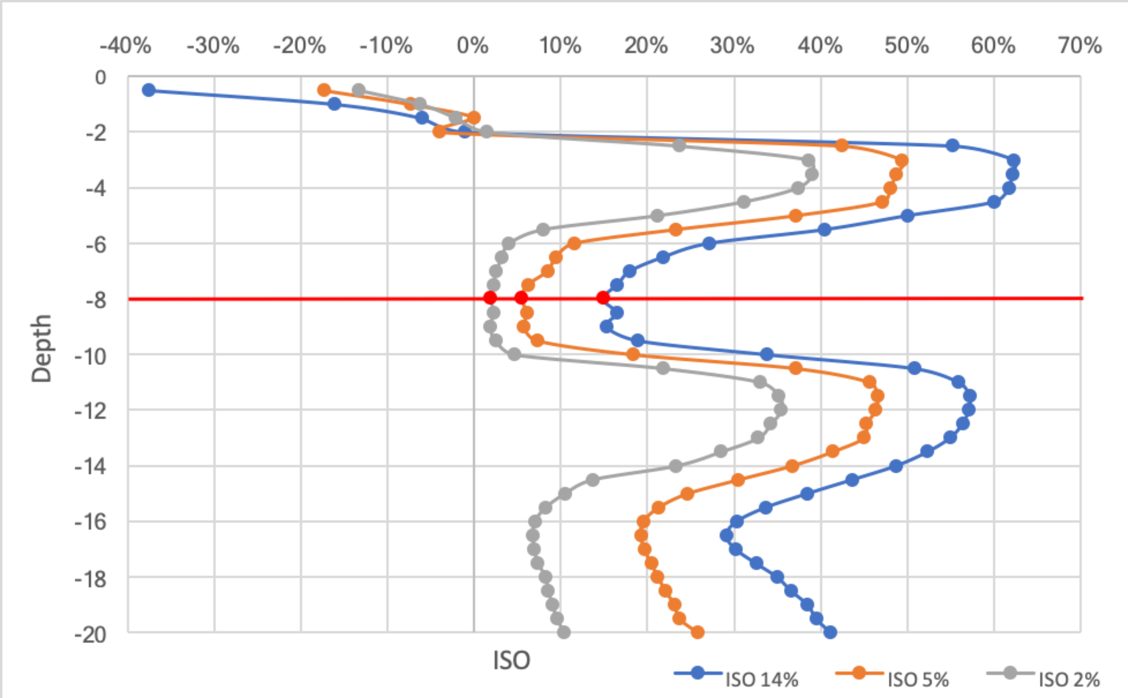

Figure 5.15. Changes in the isotropic percentages are shown with respect to manipulated hypocentral depth as a result of inversions. In this event, stations are located at 45 and 80 km distances for all the inversions. Three different cases are considered; blue lines, orange lines and blue gray expresses the moment tensor with 14%, 5% and 2% isotropy respectivelty. Moreover, red dots show the inversion results of original depth for each case and red line describes the original hypocentral depth.

When the original moment tensor has lower isotropic percentage, inverted moment tensor's isotropy value is closer to the original value at near depths to the initial depth. For instance, Figure 5.15 shows that inversion result of the moment tensor with lowest isotropy (2% iso - gray dots) gives closer values in terms of variance reduction parameters and isotropic percentages, when the manipulated depth values are closer to the initial depth (e.g 6-10 km). In other words, even if wrong hypocentral depth solutions (± 2 km) are calculated, the inversion results of the moment tensor with low isotropy give relatively correct isotropic percentages and high variance reduction values. However, in the case that moment tensor has 5% or 14% isotropy (orange and blue dots in Figure 5.15), this sensitivity is increasing. As far away from the original depth, the inversion can yield more incorrect results for earthquakes with higher isotropy.

The results for this thesis can be summarized as follows;

- The inverse solution of the moment tensor is not really sensitive to isotropy, because the isotropic component has a small amount of energy compared to the whole waveform (Figures 5.1, 5.2, 5.3,5.4, 5.5, 5.6, 5.7, 5.8, 5.9).
- Earthquakes, which has relatively high isotropic percentages, are less sensitive when inversions are made for high values of modified isotropy (Figures 5.10, 5.11, 5.12, 5.13, 5.14).
- As the altered depths move away from the original depths of earthquakes, the inversion solution for higher isotropic earthquakes may yield more incorrect results (Figure 5.15).

REFERENCES

1. Vavryčuk, V., "Tensile earthquakes: Theory, modeling, and inversion", Journal of Geophysical Research: Solid Earth, Vol. 116, No. B12, 2011.

2. Alvizuri C., Tape C., "Full moment tensors for small events (Mw ¡ 3) at Uturuncu volcano, Bolivia", Geophysical Journal International, Volume 206, Issue 3, Pages 1761–1783, 2016.

3. Pesice, J.D., Sileny J., Prejean S.G. Thurber C.H., "Determination and uncertainty of moment tensors for microearthquakes at Okmok Volcano, Alaska", Geophys. J. Int., 190, 1689–1709, 2012.

4. Panza G.F., Sarao A., "Monitoring volcanic and geothermal areas by full seismic moment tensor inversion: are non-double-couple components always artefacts of modelling?", Geophys. J. Int., 143(2), 353–364, 2000.

5. Sipkin, S. A., "Interpretation of non-double-couple earthquake mechanisms derived from moment tensor inversion", Journal of Geophysical Research: Solid Earth, Vol. 91, No. B1, pp. 531–547, 1986.

6. Jost, M. u. and R. Herrmann, "A student's guide to and review of moment tensors", Seismological Research Letters, Vol. 60, No. 2, pp. 37–57, 1989.

7. Knopoff, L. and M. J. Randall, "The compensated linear-vector dipole: A possible mechanism for deep earthquakes", Journal of Geophysical Research, Vol. 75, No. 26, pp. 4957–4963, 1970.

8. Fitch, T. J., D. W. McCOWAN and M. W. Shields, "Estimation of the seismic moment tensor from teleseismic body wave data with applications to intraplate and mantle earth- quakes", Journal of Geophysical Research: Solid Earth, Vol. 85, No. B7, pp. 3817– 3828, 1980.

9. Kuge K., Lay T., “Data-dependent non-double-couple components of shallow earthquake source mechanisms: effects of waveform inversion instability”. Geophys Res Lett. 21:9–12, 1994.

10. Julian, B.R., Miller, A.D. Foulger, G.R., “Non-double-couple earthquakes: 1”. theory, Rev. Geophys., 36, 525–549, 1998.

11. Vavryčuk, V., “Inversion for parameters of tensile earthquakes”, J. Geophys. Res., 106, No. B8, 16.339-16.355, 2001.

12. Heaton, T.H. Heaton, R.E., “Static deformation from point forces and force couples located in welded elastic Poissonian half-spaces: implications for seismic moment tensors”, Bull. seism. Soc. Am., 79, 813– 841., 1989

13. Vavryčuk, V., “Focal mechanisms in anisotropic media”, Geophysical Journal International, Vol. 161, No. 2, pp. 334–346, 2005.

14. Bóna A, Bucataru I, Slawinski MA (2007) “Coordinate-free characterization of the symmetry classes of elasticity tensors”, Journal of Elasticity 87(2-3):109–132

15. Ben-Zion,Y., “Key formulas in earthquake seismology”, International Handbook of Earthquake and Engineering Seismology, pp. 1857–1875, ed. Lee, W.H.K. Part, B., Academic Press, Boston, MA, USA, 2003.

16. Ben-Zion, Y., “On quantification of the earthquake source”, Seism. Res. Lett., 72, 151–152, 2001.

17. Zhu, Lupei Ben-Zion, Yehuda., “Parametrization of general seismic potency and moment tensors for source inversion of seismic waveform data”, Geophysical Journal International. 194. 839-843., 2013.

18. Hudson, J.A., Pearce, R.G. Rogers, R.M., “Source type plot for inversion of the moment tensor”, J. geophys. Res., 94, 765–774, 1989.

19. Chapman, C.H. Leaney, W.S., “A new moment-tensor decomposition for seismic events in anisotopic media”, Geophys. J. Int., 188, 343–370, 2012.

20. Bailey, I.W., Becker, T.W. Ben-Zion, Y., “Patterns of co-seismic strain computed from southern California focal mechanisms”, Geophys. J. Int., 177, 1015–1036, 2009

21. Aki, K. Richards, P.G., “Quantitative Seismology”, 2nd edn. University Science Books, Sausalito, CA., 2002

22. Stein, S., Wysession, M., “An introduction to seismology, earthquakes, and earth structure”, Malden, MA: Blackwell Pub., 2003.

23. Zhu, L. Helmberger, D.V., “Advancement in source estimation techniques using broadband regional seismograms”, Bull. seism. Soc. Am., 86(5), 1634–1641, 1996.

24. E. Ross, Z Ben-Zion, Y Zhu, Lupei., “Isotropic source terms of San Jacinto fault zone earthquakes based on waveform inversions with a generalized CAP method”, Geophysical Journal International. 200. 1269-1280. 10.1093/gji/ggu460, 2015.

25. Templeton, Dennise Rodgers, Arthur Helmberger, Don Dreger, Douglas., “Comparison of the Cut-and-Paste and Full Moment Tensor Methods for Estimating Earthquake Source Parameters”, AGU Fall Meeting Abstracts, 2008.

26. Aki, K. and P. G. Richards, “Quantitative Seismology: Theory and Methods”, 1980.

27. Heaton, T. H., “The 1971 San Fernando earthquake: A double event?”, Bulletin of the Seismological Society of America, Vol. 72, No. 6A, pp. 2037–2062, 1982.